UNIVERSITY OF COPENHAGEN

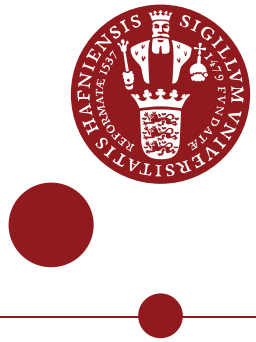

MSc in Nanoscience

Violating Bell's inequality with continuous variables & qubit-cavity interaction

Jonas Dalgaard

Supervised by Anders Søndberg Sørensen

January 2022

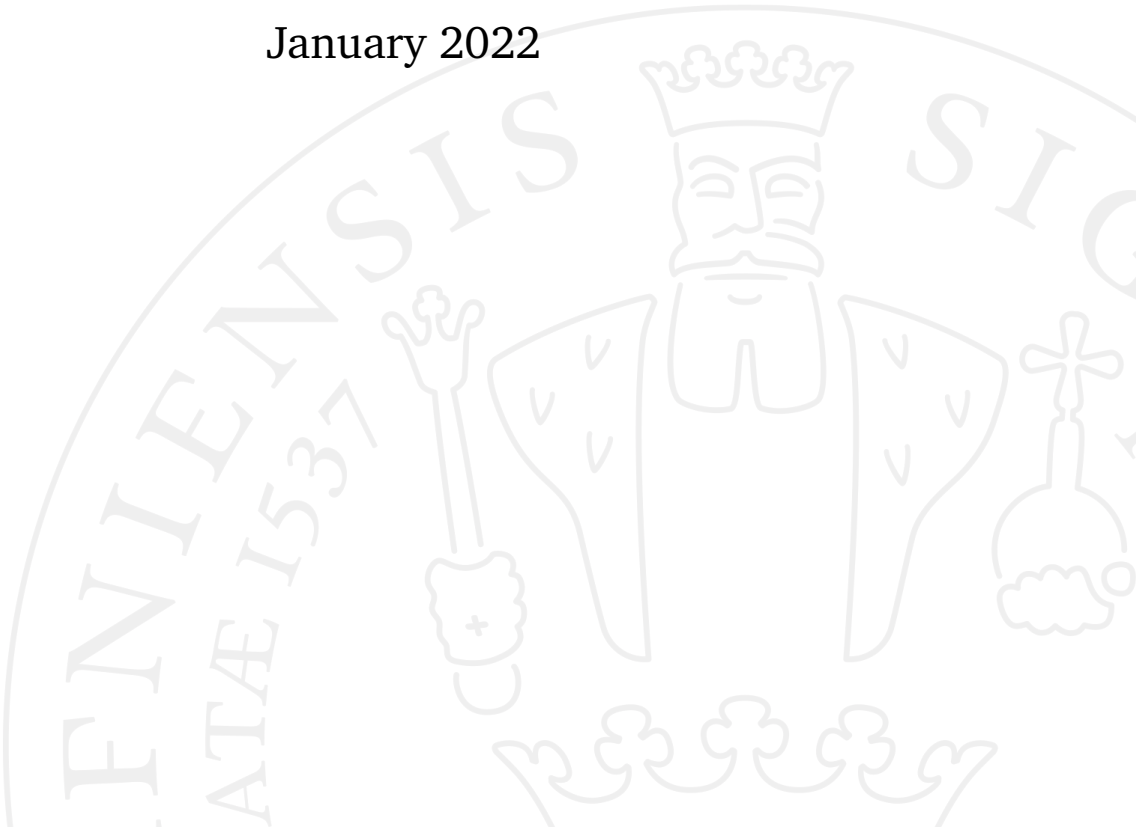

Jonas Dalgaard
Violating Bell's inequality with continuous variables & qubit-cavity interaction
MSc in Nanoscience, January 2022
Supervisor: Anders Søndberg Sørensen

University of Copenhagen
The Niels Bohr Institute
Blegdamsvej 17
2200 Copenhagen N

Acknowledgements

I would like to extend a couple of thanks for support during this project.

To Anders for eminent guidance and explanations.
To Eva for invaluable help, patience and constructive feedback.
To Nicolai for great mentoring and for helping me keep me focused.
To Begitte and Jan for helping keep me somewhat sane during this.
And to my family for putting up with incoherent explanations and rants for a year.

Abstract

A protocol for generating entangled continuous variable states violating th CHSH inequality utilizing a superconducting qubit-microwave cavity interaction is suggested. The states are adapted from an article by Wenger et. al[35] and reproduces these states differing only by a quadrature dependent phase in one term of the entangled state. In a simple theoretical setup with no noise and perfect detectors the states achieve an S value of ≈ 2.41. The protocol is iterable, allowing for the expansion of the protocol by sacrificing propability of preparing the desired state for generating a state with higher violation of the CHSH inequality.

The origin of the correlations within the prepared state is examined through the lens of subsystem decomposition, regarding them as stemming from a qubit encoded in the continuous variable states.

Contents

1 Introduction

Entangled states violating a Bell inequality are the basis for building communication setups using quantum cryptography protocols that are, in theory, completely safe from eavesdropping by unwelcome third parties[4][12]. Utilizing quantum states based on continuous variables is one potential avenue[20][38], however so far very few attempts have been able to violate the Bell tests that function as threshold for whether a state would be usable in a quantum cryptography protocol[11][30].

Advances in superconducting qubits as well as coupling of these to microwave cavities[31][21] raises the feasibility of building setups capable of violating a Bell inequality with continuous variable states of very high fidelity[18]. Kirchmair et. al. 2013[18] produced multi component cat-states of remarkably high fidelity using a superconducting Kerr-medium coupled to a microwave cavity, achieving a superposition of as much as 4 coherent states, see figure 1.1. Entangling such states seemed like a promising prospect for violating a Bell inequality and this was the initial inspiration for this project, although later the coice was made to utilize a superconducting qubit-microwave resonator interaction linking the σ_x operator of the qubit with a quadrature of the resonator phase space. The result is a protocol that generates an entangled state of continuous variables in two microwave resonators theoretically capable of violating the CHSH (Clauser-Horne-Shimony-Holt) inequality[7]. Aditionally, the protocol could be extended by repeating the initial steps before entanglement to generate more complex states with a higher violation of the CHSH inequality.

The ability of these states to violate the inequality can be better understood by doing a decomposition of the states into a logical qubit and two gauge states

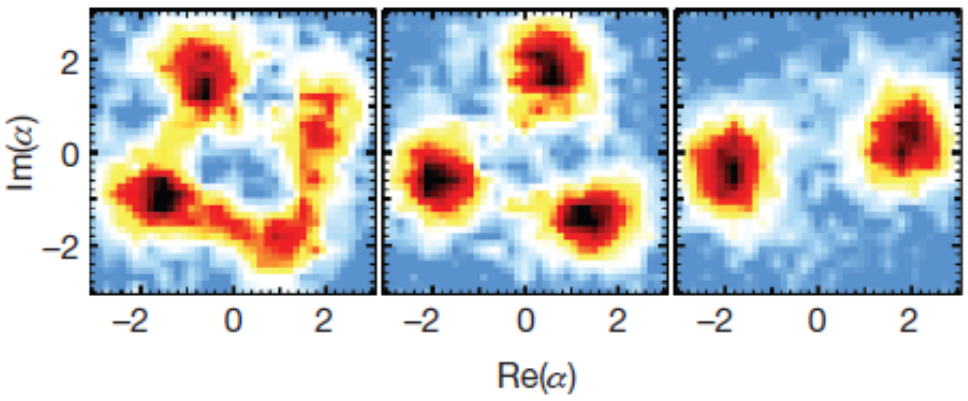

Figure 1.1: Multicomponent cat states of Kirchmair[2013][18]. The ability to prepare multicomponent coherent superpositions of high fidelity was the initial inspiration for this thesis.

i.e. as a qubit encoded within the states. This interpretation is inspired by cluster states and GKP states[13][26], leading one to hope that the applications expected of these states within quantum error correction for example could also be expected of the state prepared by this protocol.

2 Theory

2.1 Bell tests

2.1.1 Some brief history

In the early days of quantum mechanics, the philosophy of the scientific fields was one of determinism, i.e., that given precise enough instruments our ever-improving understanding of physics would eventually give us the ability to accurately predict the outcome of any physical event. The core principles of quantum mechanics flew in the face of this orthodoxy with its inherent uncertainties.

However, especially unpalatable was the concept of entanglement where a particle is only well described through its shared state with its entangled partner particle(s), in theory regardless of separation. This phenomenon that could allow a particle to instantly experience changes in its state as a result of a particle half a solar system away led Albert Einstein to infamously and mockingly dub it “spooky action at a distance”[2] (it should be noted that though entangled particles can affect each other regardless of distance, these effects do not allow for faster than light communication).

As an attempt to save their deterministic worldview but hold on to the framework of quantum mechanics, skeptics of quantum mechanics introduced the hidden variable theory[9]. This theory explained the uncertainties and strong correlations of quantum mechanics as being governed by hidden variables that allowed results to appear random in the sense asserted by quantum mechanics, but in fact be part of some distribution governed by these new variables. Similarly, entangled states would not instantaneously change when one part was manipulated, but instead have a predictable result if this new variable was known.

When John Bell proposed Bell tests, they were meant to refute local variables as an explanation of quantum phenomena[3].

2.1.2 CHSH inequality

(the derivation in this section broadly follows that found in John Preskill's unpublished book "Quantum Information and Computation" Chapter 4[27])

Two observers, Alice and Bob, are each given one of an entangled qubit pair, for example in one of the bell states

$$\left|\Phi^{+}\right\rangle = \frac{1}{\sqrt{2}}\Big(|00\rangle + |11\rangle \Big) \tag{2.1}$$

Alice can measure the observables $\mathbf{a}$ and $\mathbf{a}'$ while Bob can measure $\mathbf{b}$ and $\mathbf{b}'$, but during any given experiment they can each measure one and only one observable each. All four observables have two eigenvalues, all taking values of ± 1. What kind of correlations can we now expect from the results of Alice' and Bobs measurements? Since both $\mathbf{a}$ and $\mathbf{a}'$ have values of either $+1$ or -1, then either their sum or difference should amount to 0 and the other to ± 2. Multiplying the respective terms with $\mathbf{b}$ and $\mathbf{b}'$ we get

$$(a + a')b + (a - a')b' = \pm 2 \tag{2.2}$$

Taking expectation values and using that the expectation value of the absolute value of a variable is the upper bound of the absolute value of the expectation value, we write

$$S = |\langle ab\rangle + \langle a'b\rangle + \langle ab'\rangle - \langle a'b'\rangle| \leq 2 \tag{2.3}$$

which is the CHSH inequality[7] and limits the correlations we can expect from experiments of the type above within classical physics. However, quantum mechanics predicts cases that violate this inequality. Suppose $\mathbf{a}$ and $\mathbf{a}'$ are orthogonal operators working on Alice' qubit while $\mathbf{b}$ and $\mathbf{b}'$ are orthogonal operators working on Bobs qubit, we write these operators on the form

$$\mathbf{a}^{(\prime)} = \sigma_{\mathbf{A}} \cdot \bar{a}^{(\prime)} \tag{2.4}$$

$$\mathbf{b}^{(\prime)} = \sigma_{\mathbf{B}} \cdot \bar{b}^{(\prime)} \tag{2.5}$$

where σ_A and σ_B are eigenoperators of Alice and Bobs qubits respectively, while $\bar{a}^{(\prime)}$ and $\bar{b}^{(\prime)}$ are vectors for each observable. The expectation values in S now become

$$\langle \Phi^+ | \sigma_A \cdot \bar{a}^{(\prime)} \cdot \sigma_B \cdot \bar{b}^{(\prime)} \rangle = \cos\theta \tag{2.6}$$

with θ being the angle between $\bar{a}$ and $\bar{b}$. If $\mathbf{a}$, $\mathbf{a}'$, $\mathbf{b}$ and $\mathbf{b}'$ are coplanar and are separated by consecutive angles of $\frac{\pi}{4}$ we have

$$S = 3 \cdot \cos\frac{\pi}{4} - \cos\frac{3\pi}{4} = 2\sqrt{2} \approx 2.83 \tag{2.7}$$

so applying quantum mechanical principles to our system produces correlations exceeding those predicted by classical 'intuitive' principles. Implicit in the derivation of the inequality above is the assumption of hidden variables in the system leading to deterministic, this means that violating the CHSH inequality suggests that local-realism is not the correct description of our world.
Even with a successful Bell-test violation a local-realist might have complaints; there are several loopholes that could lead to a Bell-test being inconclusive in showing quantum mechanical correlations.
One is the locality loophole, if the two measurements aren't done very far apart or within a very short timeframe, a skeptic could rightfully claim that information about the result of the first measurement could have reached the second qubit before measurement, thus for this loophole to be closed measurements have to be separated in spacetime so information about one result travelling at spacetime cannot reach the other qubit before measurement.
Another is the detection loophole; when working with imperfect detectors with

efficiencies well below 100% a hidden variable model could feasibly favour detection results that lead to a violation of the Bell inequality even if the results with lost measurements didn't, as such detection efficiencies should be taken into account when testing hidden variable theory, though in many experiments the 'fair sampling' assumption is used, meaning that the results measured are assumed to be representative of the results that would have been achieved with 100% detector efficiency.
More loopholes exist, with most of them having been closed in experiments that achieved violation of a Bell test and with some experiments being successful with more than one loophole closed[16][28][33].

2.2 Continuous variable Bell tests

Most Bell test and in fact most quantum information experiments are done with discrete variable systems, for example for optical polarized or time binned single photons[8][22][25].
However while protocols for generating states are fairly straightforward, detection of single photons can be an issue, with efficiencies of the most common detectors, single-photon avalanche photodiodes, ranging in values between around 10 $\%$ and 65 $\%$[10][14] depending on detector and wavelength, however newer types of detectors such as superconducting nanowire single photon detector (SNSPDs) with efficiencies above 90%[37] reported. This of course leaves wide open the Bell inequality detection loophole and by extension leaves any quantum communication protocol based on these systems vulnerable to eavesdropping.
A more project specific reason to not work with single photons is the lack of options for SPDs in the microwave since we're interested in the interaction between SC qubits and microwave resonators.
Working with continuous variable states, on the other hand, allows us to use homodyne detection[15] for measurements, which in turn can use conventional photo-detectors with near unity efficiency.
The shift from discrete to continuous states also carries more inherent advantages than the ability to use conventional technology. In theory, access to continuous variables could allow for more efficient quantum computation than discrete ones. [Refs to some CV quantum computing[29][36][5]]
Since the CHSH inequality is essentially derived for a qubit with a binary result

and our continuous variables in theory can have infinitely many different results, measurement results can't be simply plugged into the inequality formula. There are two approaches to solving this, either use a different Bell inequality designed for continuous variables[6] or sort measurement results into groups and assign each group a value, so called binning, which will be our approach. The choice of binning is free and as one might expect the best choice of binning depends on the states examined, so the objective is very much to make the binning process reflect any correlations present in the states at hand. As the mention of homodyne detection suggests, the variables usually considered for continuous variable Bell tests, and indeed also here, are the quadrature operators of the electric field, $\hat{X}_1 = \frac{1}{2}(\hat{a} + \hat{a}^\dagger)$ and $\hat{X}_2 = \frac{1}{2i}(\hat{a} - \hat{a}^\dagger)$. They are orthogonal, have the commutation relation $[\hat{X}_1, \hat{X}_2] = \frac{i}{2}$, similar to that of position $\hat{x}$ and momentum $\hat{p}$, which leads to the interpretation of $\hat{X}_1$ and $\hat{X}_2$ constituting a phase space of the electric field and the convention of simply refering to them as position and momentum when working in the phase space, which will also be the case in this thesis. The infinite dimensional Hilbert spaces constituting the position and momentum variables are eigenstates of the operators and the eigenvalue problem returns the position or momentum value

$$\hat{x} \left|x\right\rangle = x \left|x\right\rangle \tag{2.8}$$

$$\hat{p} \left|p\right\rangle = p \left|p\right\rangle , \tag{2.9}$$

the postion and momentum states both form complete sets

$$\int_\infty^\infty dx \left|x\right\rangle \left\langle x\right| = 1 \tag{2.10}$$

$$\int_\infty^\infty dp \left|p\right\rangle \left\langle p\right| = 1, \tag{2.11}$$

and the fourier transform shifts between the two bases

$$\mathcal{F}(\left|x\right\rangle) \propto \int_\infty^\infty dp e^{-i2\hat{x}\hat{p}} \left|p\right\rangle \tag{2.12}$$

$$\mathcal{F}(\left|p\right\rangle) \propto \int_\infty^\infty dx e^{i2\hat{p}\hat{x}} \left|x\right\rangle . \tag{2.13}$$

Incidentally, this basis shift functions similarly to a Hadamard gate.
The displacement operators $\mathcal{D}_{\hat{x}}$ and $\mathcal{D}_{\hat{p}}$ that shift the state in $\hat{x}$ and $\hat{p}$ respectively are

$$\mathcal{D}_{\hat{x}}(X) = e^{-i2x\hat{p}} \tag{2.14}$$

$$\mathcal{D}_{\hat{p}}(p) = e^{-i2p\hat{x}}. \tag{2.15}$$

These operators also functions as phase shift operators when applied to a state of the conjugate basis.
For this project the generation of entanglement between continuous variable states is done through the interaction with a superconducting qubit, but other methods to induce correlations that have been used include Kerr mediums and two mode squeezing[11][19][34].

2.2.1 Homodyne detection

The method for measuring the quadratures $\hat{X}_1$ and $\hat{X}_2$ that constitute our continuous variables is called homodyne detection. It works by mixing the state to be measured on a beam splitter with what is conventionally called a local oscillator, a strong coherent field usually generated by the same source used for the generation of the state to be measured, thus the name homodyne; "same wave".
Suppose we have a coherent state $|\alpha\rangle$ to be measured through homodyne detection with the local oscillator $|\beta \cdot e^{-i\omega t}\rangle$ with $\beta = |\beta| \cdot e^{-i\phi}$ and the beamsplitter is a 50/50 beamsplitter meaning this would be $balanced$ homodyne detection. if the input modes are $\hat{a}$ (our state to be measured) and $\hat{b}$ (the local oscillator with output modes $\hat{c}$ and $\hat{d}$, the transformation through the beam splitter is

$$\begin{pmatrix} \hat{c} \\ \hat{d} \end{pmatrix} = \frac{1}{\sqrt{2}} \begin{pmatrix} 1 & i \\ i & 1 \end{pmatrix} \cdot \begin{pmatrix} \hat{a} \\ \hat{b} \end{pmatrix}. \tag{2.16}$$

Following the beam splitter, two detectors measure the intensities $I_\sigma = \langle \hat{\sigma}^\dagger \hat{\sigma} \rangle$ of modes $\hat{c}$ and $\hat{d}$, leading to the shared measurement of the difference of intensities

$$I_c - I_d = \langle \hat{c}^\dagger \hat{c} - \hat{d}^\dagger \hat{d} \rangle = \langle \hat{a}^\dagger \hat{b} - \hat{b}^\dagger \hat{a} \rangle. \tag{2.17}$$

We can now move the magnitude $|\beta|$ out and, assuming $|\alpha\rangle$ also has frequency ω, the time dependency cancels out. $|\beta\rangle$ picks up a phase of $\frac{\pi}{2}$ so defining $\theta = \phi + \frac{\pi}{2}$ we have

$$I_c - I_d = |\beta| \cdot \langle \hat{a}^\dagger e^{-i\omega t} e^{i\theta} + \hat{a} e^{i\omega t} e^{-i\theta} \rangle = 2|\beta| \langle \hat{X}(\theta) \rangle, \tag{2.18}$$

with

$$\hat{X}(\theta) = \frac{1}{2}\left(\hat{a}_0 e^{-i\theta} + \hat{a}_0^\dagger e^{i\theta} \right). \tag{2.19}$$

So through the choice of local oscillator, the quadrature being measured can be chosen with a given angle, the position and momentum quadratures are

$$\hat{X}_1 = \hat{X}(0) \tag{2.20}$$

$$\hat{X}_2 = \hat{X}(\frac{\pi}{2}). \tag{2.21}$$

2.3 Wenger et. al. 2003

In a 2003 paper[35] Wenger et. al. proposed a theoretical CV scheme that could produce values of the CHSH inequality arbitrarily close to the maximum of $2\sqrt{2}$ using an on the surface simple binning scheme and a superposition of multi component coherent states. However, at the time the authors deemed their proposal infeasible mainly due to the lack of a realistic way of implementing certain parts of their protocol (specifically a coupling Hamiltonian

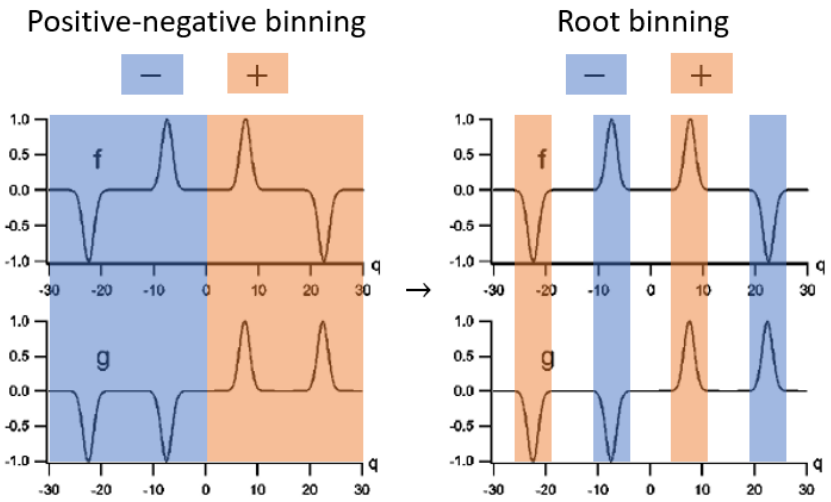

Figure 2.1: Left: A simple scheme one might come up with for an arbitrary state sorting quadrature measurements according to whether the result came out positive or negative, for example used in my early attempts with Kerr induced cat states (see chapter 6.1). Right: The rootbinning scheme. Quadrature measurements are sorted into bins according to whether $|f\rangle$ and $|g\rangle$ have the same or different sign in a given area.

and a CNOT-gate). This combination of states and binning quickly became my blueprint for getting from SC qubit coupling to CV states capable of violating a Bell inequality. Early on during the project I chose to pursue the states proposed in this paper, hoping that a superconductor-microwave cavity interaction would prove to be the missing piece of the puzzle. The wave function is an even superposition of the states introduced in the article

$$|\Psi\rangle = \frac{1}{\sqrt{2}}\Big(|ff\rangle + e^{i\theta}\,|gg\rangle \Big), \tag{2.22}$$

with $|f\rangle$ and $|g\rangle$ being the even and odd functions described below. The binning scheme introduced is coined “root binning” (see figure 2.1), translating the continuous variable measurement obtained to a binary result necessary to calculate the CHSH inequality by sorting results according to whether they fall within areas of same or differing signs for the functions f and g described below. Results sorted into the + bin (same sign) are assigned the value +1 while results sorted in the – (differing sign) are assigned -1. With results sorted S can be calculated as for a discrete system. In the article, two infinite sums of delta functions are considered

$$f_{\inf}(x,\alpha) \propto \sum_{j=-\infty}^{\infty} \cos\left(\frac{\pi x}{2\alpha}\right)\delta\Big(x - 2(j+\frac{1}{2})\alpha\Big) \tag{2.23}$$

$$g_{\inf}(x,\alpha) \propto \sum_{j=-\infty}^{\infty} \sin\left(\frac{\pi x}{2\alpha}\right)\delta\Big(x - 2(j+\frac{1}{2})\alpha\Big) \tag{2.24}$$

the main difference is their symmetry around 0, with f being even and g being odd. Another interesting property is that they for $\alpha = \sqrt{\pi}$ they are (apart from a scaling constant) identical to their fourier transforms. This along with the fact that f and g overlap perfectly suggests that very strong correlations can be expected. These states are of course unphysical because of both the infinite number and narrowness of the peaks. More reasonable functions with limited number of peaks and delta functions widened out to gaussians

$$f_N(x,\alpha) \propto \sum_{j=-(N/2)}^{(N/2)} \cos\Big(\frac{\pi}{4}(2j+1)\Big) \cdot e^{-\left(x-2(j+\frac{1}{2})\alpha\right)^2/2} \tag{2.25}$$

$$g_N(x,\alpha) \propto \sum_{j=-(N/2)}^{(N/2)} \sin\Big(\frac{\pi}{4}(2j+1)\Big) \cdot e^{-\left(x-2(j+\frac{1}{2})\alpha\right)^2/2}. \tag{2.26}$$

For 4 peaks these become

$$f(x,\alpha) \propto -e^{-(x+3\alpha)^2/2} + e^{-(x+\alpha)^2/2} + e^{-(x-\alpha)^2/2} - e^{-(x-3\alpha)^2/2} \tag{2.27}$$

$$g(x,\alpha) \propto -e^{-(x+3\alpha)^2/2} - e^{-(x+\alpha)^2/2} + e^{-(x-\alpha)^2/2} + e^{-(x-3\alpha)^2/2}. \tag{2.28}$$

To calculate S, the probability of different measurement outcomes as sorted within the bins described above must first be calculated

$$P_{\pm\pm} = \int_{D^\pm}\int_{D^\pm} d\sigma_A d\sigma_B \Psi(\sigma_A,\sigma_B) \tag{2.29}$$

with $\Psi(\sigma_A,\sigma_B)$ being the wavefunction in the corresponding bases σ_A and σ_B, and $D^\pm$ denoting group of bins to be integrated over. The corresponding correlation function is then

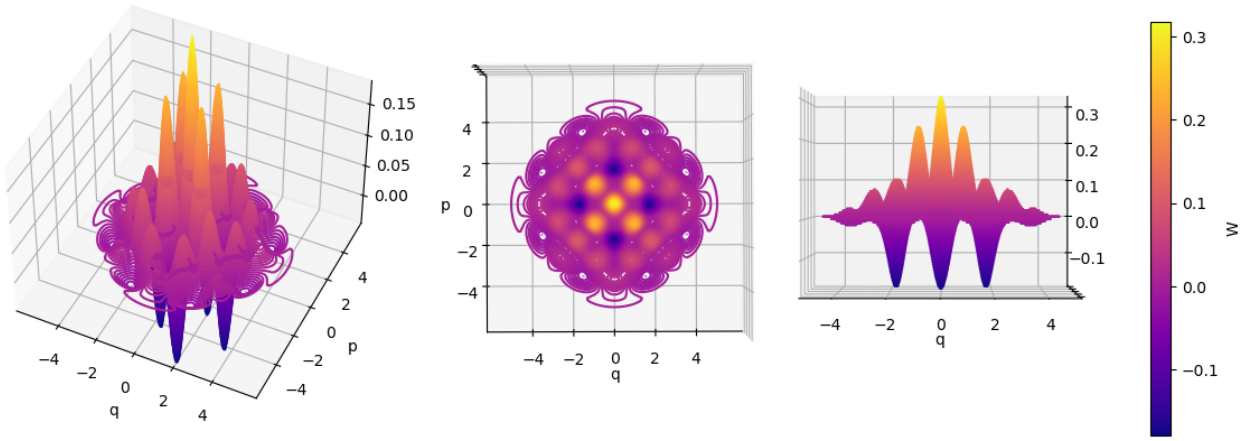

(a)

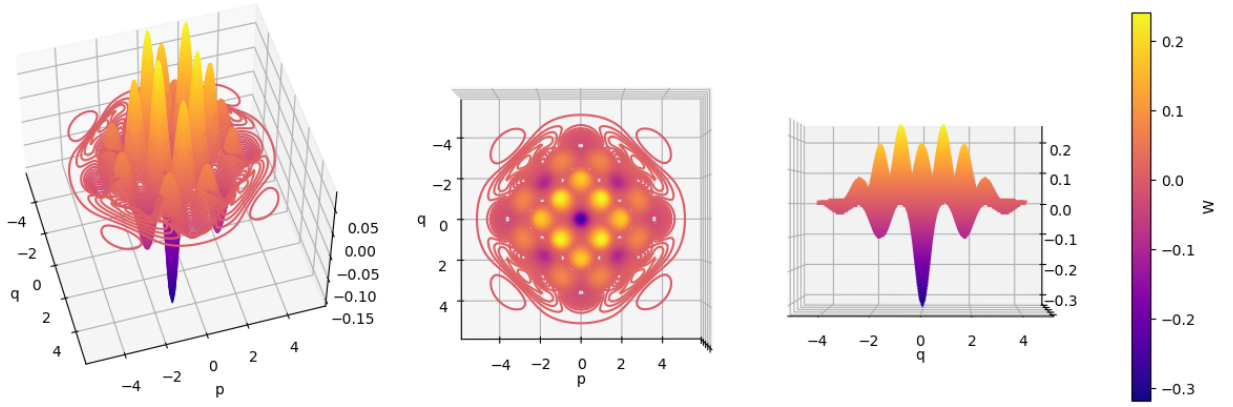

(b)

Figure 2.2: Plots of the Wigner functions of (a) $|f\rangle$ and (b) $|g\rangle$, although the states have been approximated with superpositions of Fock states given in [35]. Plots are done using the python package QuTip[17].

$$E_{\sigma_A\sigma_B} = P_{++} + P_{--} - P_{+-} - P_{-+}. \tag{2.30}$$

Finally, the CHSH inequality is calculated as

$$S = |E_{xx} + E_{px} + E_{xp} - E_{pp}| \leq 2. \tag{2.31}$$

Because of f and g being even and odd respectively, a simpler expression for S can be reached with some clever rewriting

$$S = |\cos(\theta)\left(W^2 + V^2\right) - 2\sin(\theta)WV| \tag{2.32}$$

with

$$V = \int_{D^+} f(x)g(x)dx - \int_{D^-} f(x)g(x)dx = \int_{-\infty}^{\infty} |f(x)g(x)|dx \tag{2.33}$$

$$W = \int_{D^+} \tilde{f}(p)\tilde{g}(p)dp - \int_{D^-} \tilde{f}(p)\tilde{g}(p)dp = \int_{-\infty}^{\infty} |\tilde{f}(p)\tilde{g}(p)|dp, \tag{2.34}$$

where $\tilde{f}(p)$ and $\tilde{g}(p)$ are the Fourier transform of $f(x)$ and $(g(x))$. This periodic function reaches its maximum at $\theta = \frac{-\pi}{4}$ and tends towards the maximum violation possible of $S = 2\sqrt{2}$ as number of peaks goes towards ∞. Some results from the article can be seen in [figure] and [table], showing the increased violation with increased number of peaks and α.

2.4 Coupling of σ_x to $\hat{x}$

Here follows a very brief summation of the derivation of the $\hat{\sigma}_x\hat{x}$ operator[32]. By driving the system on resonance, the interaction can be shown through rotating wave approximation to be express-able on the form $\mathcal{H} \propto \hat{\sigma}_x\hat{x}$. The

Hamiltonian for the interaction between the external driving field and the qubit-cavity system can be written as

$$\mathcal{H} = \hbar\omega_c \hat{a}^\dagger \hat{a} + \frac{\hbar\omega_q}{2}\hat{\sigma}_z + \hbar g \hat{\sigma}_x(\hat{a}^\dagger + \hat{a}) - \vec{d}\cdot\vec{E}, \tag{2.35}$$

with ω_c being the frequency of the cavity mode and $\hbar\omega_q$ being the qubit energy spacing. $\vec{d} = \vec{d}_{eg}\left|e\right\rangle\left\langle g\right| + \vec{d}^*_{eg}\left|g\right\rangle\left\langle e\right|$ is the dipole vector, $\vec{E} = \vec{E}_0 e^{-i\omega_L t} + \vec{E}_0^* e^{i\omega_L t}$ is the driving field and ω_L the laser frequency and g is the coupling constant. Shifting to the interaction picture the interaction part of the Hamiltonian can be written as

$$\begin{aligned}\mathcal{H}_I = \hbar\Delta a^\dagger a + \frac{\hbar\delta}{2}\hat{\sigma}_z + \hbar g\Big(\hat{\sigma}_+ a^\dagger e^{i2\omega_L t} + \hat{\sigma}_- a^\dagger + \hat{\sigma}_+ a + \hat{\sigma}_- a e^{-i2\omega_L t}\Big) \\ + \Big(\hbar\frac{\Omega}{2} + \hbar\frac{\Omega}{2}e^{i2\omega_L t}\Big)\hat{\sigma}_+ + \Big(\hbar\frac{\Omega^*}{2} + \hbar\frac{\Omega^*}{2}e^{-i2\omega_L t}\Big)\hat{\sigma}_-,\end{aligned} \tag{2.36}$$

where $\Delta = \omega_c - \omega_L$, $\delta = \omega_q - \omega_L$ and $\frac{\Omega}{2} = -\vec{d}\cdot\vec{E}$. The rotating wave approximation is then applied, discarding rapidly oscillating terms that can be taken to average to 0 on the timescale of any interaction we're interested in.

$$\mathcal{H}_I = \hbar\Delta a^\dagger a + \frac{\hbar\delta}{2}\hat{\sigma}_z + \hbar g\Big(\hat{\sigma}_- a^\dagger + \hat{\sigma}_+ a\Big) + \hbar\frac{\Omega}{2}\hat{\sigma}_x, \tag{2.37}$$

assuming $\omega_L \gg g, \Omega, \Delta, \delta$. Finally the interaction Hamiltonian is expressed in a rotating frame by applying the unitary transformation

$$U \equiv e^{-i\frac{\Omega}{2}\hat{\sigma}_x t}, \tag{2.38}$$

yielding

$$\mathcal{H}_I' = U^\dagger \mathcal{H}_I U = e^{i\frac{\Omega}{2}\hat{\sigma}_x t}\Big(\hbar\Delta a^\dagger a + \frac{\hbar\delta}{2}\hat{\sigma}_z + \hbar g\Big(\hat{\sigma}_- a^\dagger + \hat{\sigma}_+ a\Big) + \hbar\frac{\Omega}{2}\hat{\sigma}_x\Big)e^{-i\frac{\Omega}{2}\hat{\sigma}_x t}, \tag{2.39}$$

the resulting expression can be simplified greatly by assuming $\Omega \gg g, \Delta$, which is ensured by driving the interaction with a strong laser, followed by another rotating wave approximation, again disregarding rapidly oscillating terms, yielding

$$\mathcal{H}_I' = \hbar\Delta a^\dagger a + \hbar\frac{g}{2}(a^\dagger + a)\sigma_x$$

which for resonance $\Delta = 0$ becomes

$$\mathcal{H}_I' = +\hbar\frac{g}{2}(a^\dagger + a)\sigma_x.$$

This is the interaction operator that turns out to be useful in the generation of the desired states.

Results

3

3.1 Protocol for generating states

The purpose of this protocol is to generate 4 peak versions of the states of [35], a sketch of the $\hat{x}$ basis plots of the states ($|f\rangle$ and $|g\rangle$) can be seen in figure 3.2. The setup consists of two modes, each consisting of a microwave cavity coupled to a superconducting qubit. In addition, both modes are coupled to the same additional SC qubit used in the generation of the entanglement, see figure 3.1. Initially both cavity fields are in the vacuum state $|\emptyset\rangle$ and the qubits are in an equal superposition in the $\hat{x}$ basis

$$|\psi_{qubit}\rangle = \frac{1}{\sqrt{2}}(|+\rangle + |-\rangle). \tag{3.1}$$

Utilizing the $\hat{\sigma}_x\hat{x}$ interaction operator the first two peaks can be formed, the operator has the form

$$e^{i\sigma_x\ \hat{x}t/\hbar} \tag{3.2}$$

with $\hat{x} = \frac{1}{\sqrt{2}}(\hat{a}^\dagger + \hat{a})$ and $\sigma_x = \begin{pmatrix} 0 & 1 \\ 1 & 0 \end{pmatrix}$. Since the state of the qubit is in the $\hat{x}$ basis, with the states $|+\rangle = \frac{1}{\sqrt{2}}(|0\rangle + |1\rangle)$ and $|-\rangle = \frac{1}{\sqrt{2}}(|0\rangle - |1\rangle)$ having eigenvalues of ± 1 respectively, the effect of $\hat{\sigma}_x$ on the composite cavity-qubit system in the $\hat{x}$ basis is simply a sign dependent on the qubit being in either the $|+\rangle$ or $|-\rangle$ state. The rest off the operator can be rewritten as a displacement operator in the following way

$$e^{i\frac{1}{\sqrt{2}}(\hat{a}^\dagger+\hat{a})t/\hbar} = e^{\frac{it}{\hbar\sqrt{2}}(\hat{a}^\dagger+\hat{a})} = e^{\frac{it}{\hbar\sqrt{2}}\hat{a}^\dagger - \frac{it}{\hbar\sqrt{2}}\hat{a}} = D\Big(\frac{it}{\hbar\sqrt{2}}\Big). \tag{3.3}$$

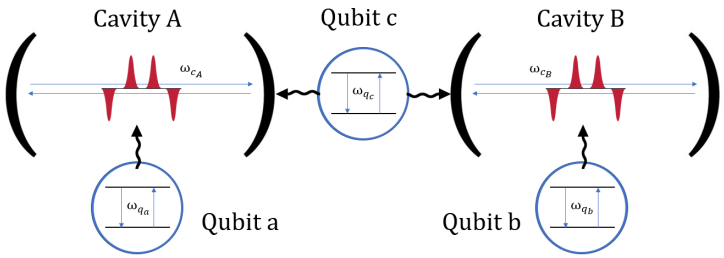

(a)

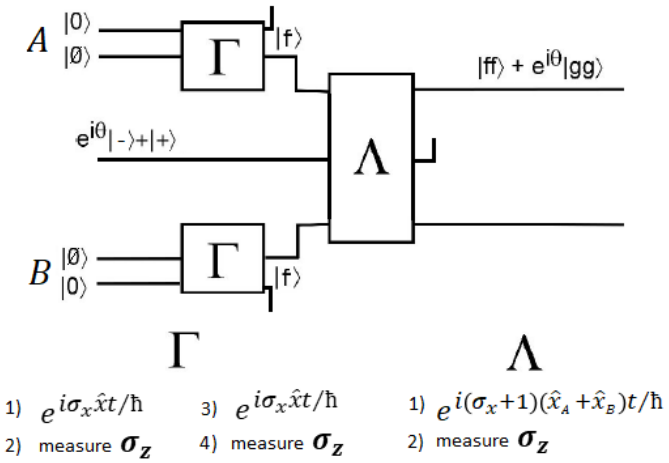

(b)

Figure 3.1: Two different views of the system. Two qubits are used in the preparation of the local states in the cavities, while a third (coupled to both cavities) is used to entangle the states in the cavities.(a) Overview of the interactions between the different subsystems. (b) Schematic of the setup adapted from [35] with overview of what subsystems the different parts of the protocol affect, Γ preparing the individual cavity fields in the desired states through two applications of the $\hat{\sigma}_x\hat{x}$ operator (1) and 3)) and two measurements of $\hat{\sigma}_z$ (2) and 4)) and λ entangling the states of the cavity fields through the application of the entangling operator and a measurement of $\hat{\sigma}_z$.

So applying the interaction operator to the initial state of either mode of the setup we get

$$\begin{aligned} & e^{i\sigma_x \hat{x} t/\hbar}\Big(\frac{1}{\sqrt{2}}(|+\rangle + |-\rangle\Big)\,|\emptyset\rangle \\ &= \frac{1}{\sqrt{2}}\Big(D\big(\frac{it}{\hbar\sqrt{2}}\big)\,|+\rangle\,|\emptyset\rangle + D\big(-\frac{it}{\hbar\sqrt{2}}\big)\,|-\rangle\,|\emptyset\rangle\Big), \end{aligned} \tag{3.4}$$

and by choosing $\frac{t}{\hbar\sqrt{2}} = 2\alpha$ we have

$$\frac{1}{\sqrt{2}}(|+\rangle\,|i2\alpha\rangle + |-\rangle\,|-i2\alpha\rangle). \tag{3.5}$$

(Equations 3.4 and 3.5 correspond to step 1 of Γ in figure 3.1(b).)
We now have a cat state, however the state of the cavity field is entangled with that of the qubit. Another application of the interaction operator is needed to go from 2 to 4 peaks, but first the cavity and qubit states must be disentangled. To this end a measurement along $\hat{\sigma}_z$ is made

$$\begin{aligned} & \hat{\sigma}_z(|+\rangle\,|i2\alpha\rangle + |-\rangle\,|-i2\alpha\rangle) \\ &= \hat{\sigma}_z(|0\rangle + |1\rangle)\,|i2\alpha\rangle + (|0\rangle - |1\rangle)\,|-i2\alpha\rangle \\ &= \begin{cases} |i2\alpha\rangle\,|0\rangle \\ -\,|-i2\alpha\rangle\,|1\rangle \end{cases} = \pm\,|i2\alpha\rangle \pm |-i2\alpha\rangle)(|+\rangle \pm |-\rangle), \end{aligned} \tag{3.6}$$

corresponding to step 2 of γ in (b) of figure 3.1.
The interaction operator is then applied again, this time choosing $\frac{t}{\hbar\sqrt{2}} = \alpha$

$$\begin{aligned} & \pm e^{i\sigma_x \hat{x}\alpha}(|i2\alpha\rangle \pm |-i2\alpha\rangle)\,|+\rangle \pm |-\rangle) \\ &= \pm(|i3\alpha\rangle\,|+\rangle \pm |i\alpha\rangle\,|-\rangle \pm |-i\alpha\rangle\,|+\rangle + |-i3\alpha\rangle\,|-\rangle), \end{aligned} \tag{3.7}$$

corresponding to step 3 of γ in (b) of figure 3.1.
A measurement along $\hat{z}$ is then made

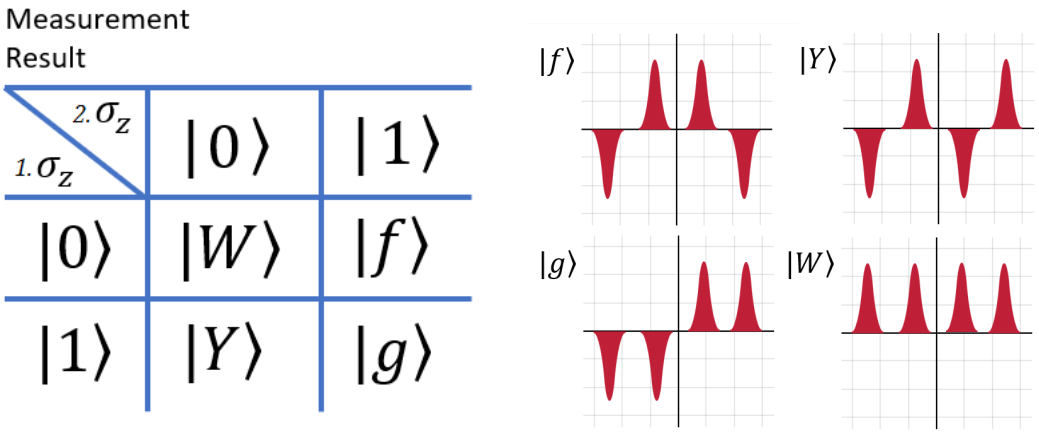

(a) (b)

Figure 3.2: Measurement dependent results of the protocol.

$$\begin{aligned}&\hat{\sigma}_z(\pm(|i3\alpha\rangle|+\rangle \pm |i\alpha\rangle|-\rangle \pm |-i\alpha\rangle|+\rangle + |-i3\alpha\rangle|-\rangle)\\ &= \begin{cases}\pm(|i3\alpha\rangle \pm |i\alpha\rangle \pm |-i\alpha\rangle + |-i3\alpha\rangle)|0\rangle\\ \pm(|i3\alpha\rangle \mp |i\alpha\rangle \pm |-i\alpha\rangle - |-i3\alpha\rangle)|1\rangle\end{cases}.\end{aligned} \tag{3.8}$$

The resulting state is an array of 4 coherent states with phases determined by the results of the qubit measurements, as can be seen in figure 3.2. Since we're looking for an even superposition in the final state and since either mode has 4 potential outcomes the protocol, we have a 1/16 chance of preparing the desired state before entanglement is generated with the shared qubit. In theory either $|ff\rangle$ or $|gg\rangle$ will work for generating the entangled state $|\Psi\rangle = \frac{1}{\sqrt{2}}(|ff\rangle + e^{i\theta}|gg\rangle$, however the phase θ between the two states of the superposition is introduced through the shared qubit Due to technical limitations, mainly coherence time of the states versus the time required to measure the one mode qubits and prepare the shared qubit, this phase has to be chosen ahead of time. Thus only either $|ff\rangle$ or $|gg\rangle$, depending on the chosen phase, will produce a state that will violate the CHSH inequality, at least within the proposed scheme. Assuming $|gg\rangle$ has been prepared and the shared qubit is prepared in the state $\frac{1}{\sqrt{2}}(|+\rangle + e^{i\theta}|-\rangle)$, we proceed with the entangling operator (step 1 of Λ in (b) of figure 3.1)

$$e^{i(\sigma_x+1)/\sqrt{2}(\hat{x}_A+\hat{x}_B)t/\hbar}. \tag{3.9}$$

Acting with this operator on the state described above, σ_x applied to the qubit state returns an eigenvalue of ± 1, so $(\hat{\sigma}_x + 1)$ will equal either 0 or 2, meaning the entire operator acts trivially when applied to a state of the cavity which is coupled to the $|-\rangle$ state of the qubit. For the $|+\rangle$ state where the first parenthesis no longer sums to zero, a rewriting similar to the single cavity case can be used. Since the operators $\hat{x}_A$ and $\hat{x}_B$ commute the exponential can be split into two, separating the operator for either cavity

$$e^{i\sqrt{2}(\hat{x}_A+\hat{x}_B)t/\hbar} = e^{\frac{i\sqrt{2}t}{\hbar}\hat{x}_A)} e^{\frac{i\sqrt{2}t}{\hbar}\hat{x}_B)}, \tag{3.10}$$

we can now apply these to the respective modes, choosing the time $(t\sqrt{2})/\hbar = \pi/2\alpha$, the effect is then a position dependent phase on the states of both cavities. For now, we will use the approximation that peaks acquire the same phase for the whole gaussian that describes it, determined by its mean. This is a good approximation for large α, but it will be corrected later nonetheless. In this approximation each cavity can now be evaluated separately applying the corresponding part of the operator

$$\begin{aligned} & e^{\frac{i\sqrt{2}t}{\hbar}\hat{x}}(+|3\alpha\rangle + |\alpha\rangle - |-\alpha\rangle - |-3\alpha\rangle) \\ = e^{i3\pi/2} & |3\alpha\rangle + e^{i\pi/2}|\alpha\rangle - e^{-i\pi/2}|-\alpha\rangle - e^{-i3\pi/2}|-3\alpha\rangle \\ & = -i|3\alpha\rangle + i|\alpha\rangle + i|-\alpha\rangle - i|-3\alpha\rangle = i|f\rangle \end{aligned} \tag{3.11}$$

so the interaction operator has the following effect when applied to the state prepared in the two cavities and the shared qubit described above

$$\begin{aligned} & e^{\frac{i(\sigma_x+1)}{\sqrt{2}}(\hat{x}_A+\hat{x}_B)t/\hbar}|gg\rangle \frac{1}{\sqrt{2}}(|+\rangle + |-\rangle) \\ & = \frac{1}{\sqrt{2}}(i^2|ff\rangle|+\rangle + e^{i\theta}|gg\rangle|-\rangle) \end{aligned} \tag{3.12}$$

To separate the states of the cavities from the shared qubit a measurement along $\hat{z}$ is made (step 2 of Λ in (b) of figure 3.1)

$$\begin{aligned}
&\frac{1}{\sqrt{2}}(-\left|ff\right\rangle\left|+\right\rangle+e^{i\theta}\left|gg\right\rangle\left|-\right\rangle)= \\
&\frac{1}{\sqrt{2}}(-\left|ff\right\rangle(\left|0\right\rangle+\left|1\right\rangle)+e^{i\theta}\left|gg\right\rangle(\left|0\right\rangle-\left|1\right\rangle) \\
&=\begin{cases}\frac{1}{2}(-\left|ff\right\rangle+e^{i\theta}\left|gg\right\rangle)\left|0\right\rangle \\ \frac{1}{2}(-\left|ff\right\rangle+e^{i\theta}\left|gg\right\rangle)\left|1\right\rangle\end{cases}.
\end{aligned} \tag{3.13}$$

The measurement dependent sign may seem troublesome, but luckily the Bell inequality can still be violated regardless of this sign if the right θ is chosen since the dependency of S on θ is periodic with a periodicity of π. Thus, the protocol prepares the 4-peak state of Wenger et. al. 2003 with a probability of 1/16, with an overall phase and potentially an internal phase that doesn't impact results.

This result was obtained assuming that the position operator $\hat{x}$ applied to a coherent state is well approximated by multiplying a single phase onto the state, however without this approximation we expect a position dependent phase.

Going back to the operator partitioned into cavity specific exponentials and again choosing $(t\sqrt{2})/\hbar = \pi/2\alpha$, we can write the exponential as a real cosine and an imaginary sine

$$\begin{aligned}
&e^{\frac{i\pi}{2\alpha}\hat{x}_B t}(\left|i3\alpha\right\rangle+\left|i\alpha\right\rangle-\left|-i\alpha\right\rangle-\left|-i3\alpha\right\rangle) \\
&=(\cos\left(\frac{\pi}{2\alpha}x_B t\right)+i\sin\left(\frac{\pi}{2\alpha}\hat{x}_B t\right))(\left|i3\alpha\right\rangle+\left|i\alpha\right\rangle-\left|-i\alpha\right\rangle-\left|-i3\alpha\right\rangle).
\end{aligned} \tag{3.14}$$

With the chosen time, the contents of the trigonometric functions will equal either $\pi/2$ or $3\pi/2$ at the peaks, meaning that the cosine will be approximately 0 and the sine will be approximately ± 1, meaning the imaginary part is approximately equal to $\left|f\right\rangle$ and in fact going towards $\left|f\right\rangle$ as $\alpha \to \infty$, meanwhile we have a real cosine part going towards 0 as $\alpha \to \infty$, see figure 3.3.

To find out how the entangling operator affects the wavefunctions of the states in the momentum basis, we do the Fourier transform of the $\hat{x}$ basis wavefunctions to find those of the $\hat{p}$ basis, for $\left|g\right\rangle$ we have

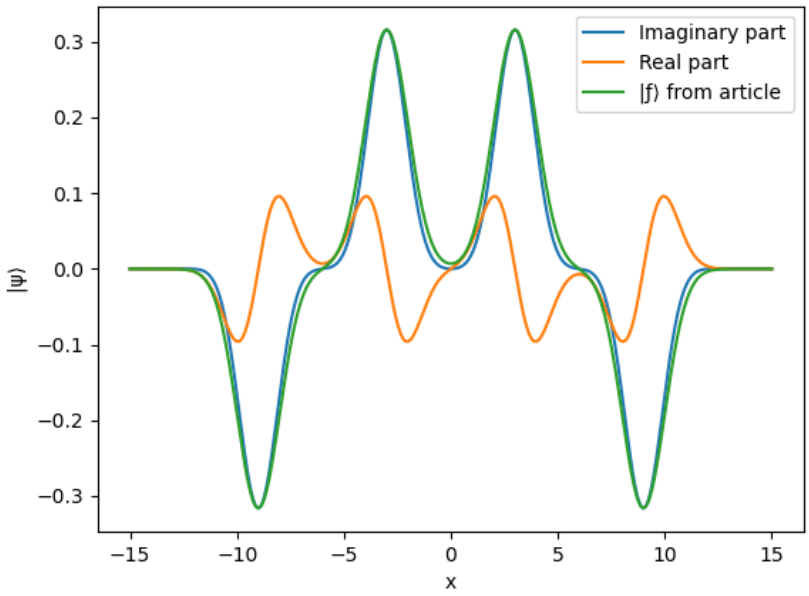

(a)

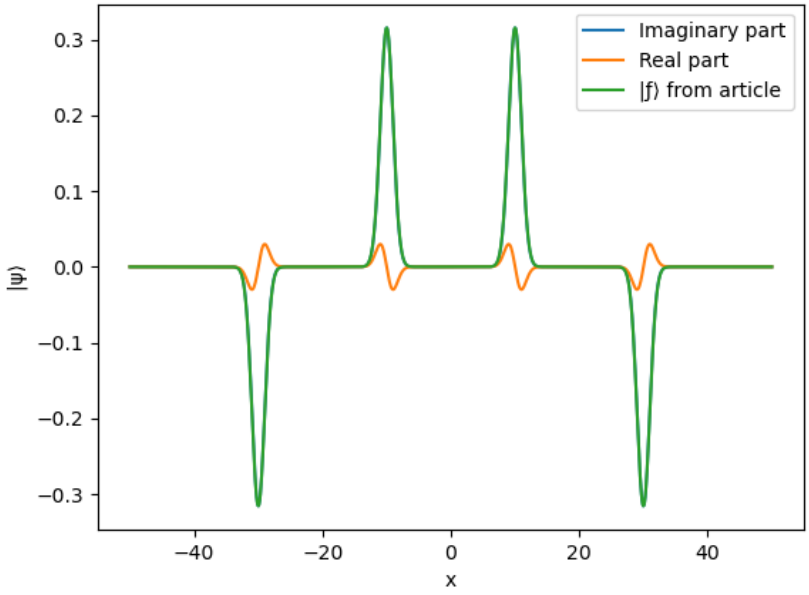

(b)

Figure 3.3: Comparison of $|f_{protocol}\rangle$ (real and imaginary parts) and $|f_{article}\rangle$ for (a) $\alpha = 3$ and (b) $\alpha = 10$. As α increases the imaginary part dies out and the state produced by the protocol becomes all but indistinguishable from the desired state.

$$\begin{aligned}
&\mathfrak{F}(e^{-(x+3\alpha)^2/2} + e^{-(x+\alpha)^2/2} - e^{-(x-\alpha)^2/2} - e^{-(x-3\alpha)^2/2}) \\
&= \frac{1}{\sqrt{2\pi}} e^{-(\pi^2\ p^2)/2}(e^{-i6\alpha\pi p} + e^{-i2\alpha\pi p} - e^{i2\alpha\pi p} - e^{i6\alpha\pi p}) \\
&= -i\sqrt{\frac{2}{\pi}} e^{(-(\pi^2\ p^2)/2)}(sin(6\alpha\pi p) + sin(2\alpha\pi p)).
\end{aligned} \tag{3.15}$$

So in the $\hat{p}$ basis we have a sum of sine functions with a gaussian envelope function. For the approximate $|f\rangle$ state produced by the operator on the $|g\rangle$ state, with the Fourier transform of the $\hat{x}$ basis function we have

$$\mathfrak{F}((e^{\frac{i\pi}{2\alpha}\hat{x}_B})(e^{-(x+3\alpha)^2/2} + e^{-(x+\alpha)^2/2} - e^{-(x-\alpha)^2/2} - e^{-(x-3\alpha)^2/2})) \tag{3.16}$$

and for Fourier transforms of the product of functions we have

$$\mathfrak{F}(f(x) \cdot g(x)) = \mathfrak{F}(f(x)) * \mathfrak{F}(g(x)) \tag{3.17}$$

where $*$ denotes the convolution of the two functions. For the Fourier transform of an exponential of this form we have

$$\mathfrak{F}(e^{ikx}) = \delta(p - k/2\pi) \tag{3.18}$$

and for the convolution of a function with a delta function we can use the sifting property

$$\int_{-\infty}^{\infty} f(t)\delta(t - T)dt = f(T) \tag{3.19}$$

from which follows

$$f(t) * \delta(t - T) = \int_{-\infty}^{\infty} f(\tau)\delta(t - T - \tau)d\tau = f(t - T) \tag{3.20}$$

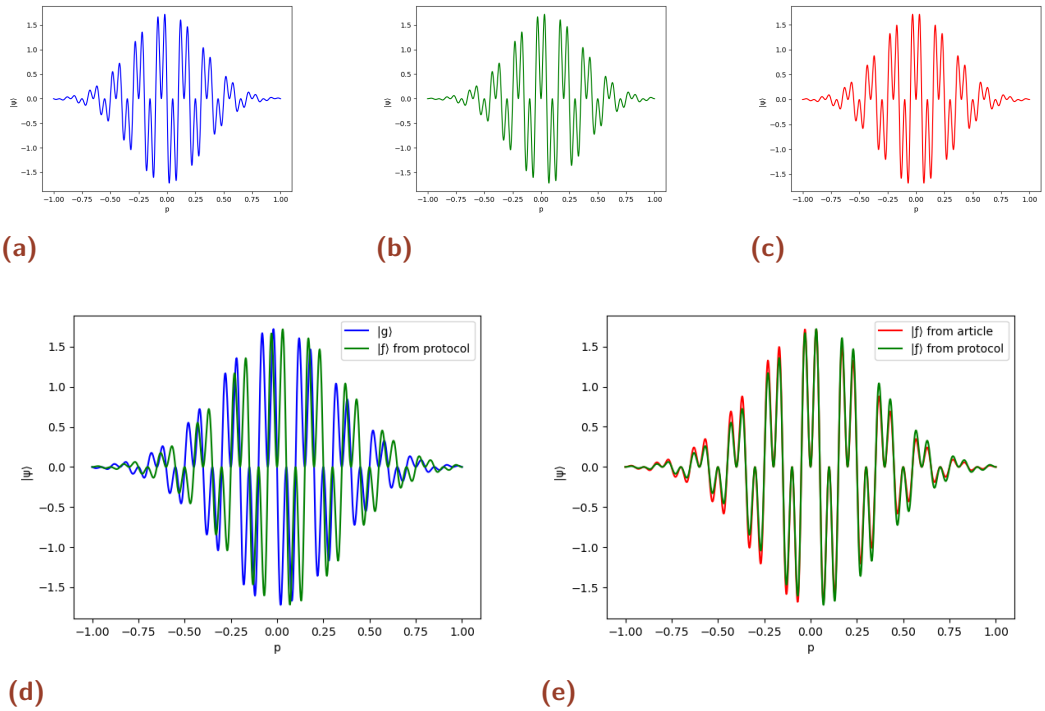

Figure 3.4: Wavefunctions for the $\hat{p}$ basis of (a) $|g\rangle$, (b)$|f_{protocol}\rangle$,(c) and $|f_{article}\rangle$. Comparisons between (d)$|g\rangle$ and $|f_{protocol}\rangle$, note that the states are identical except for a shift in $\hat{p}$, (e) $|f_{protocol}\rangle$ and $|f_{article}\rangle$, the states share roots and local extrema, but the Gaussian envelope is shifted.

so for $|f\rangle_{approx}$ (eq 3.16) we get

$$\begin{aligned}
&\mathfrak{F}\Big(e^{(i\pi/2\alpha)\hat{x}_B}\big(e^{-(x+3\alpha)^2/2}+e^{-(x+\alpha)^2/2}-e^{-(x-\alpha)^2/2}-e^{-(x-3\alpha)^2/2}\big)\Big)\\
&=\delta(p-\frac{1}{4\alpha})*\frac{1}{\sqrt{2\pi}}e^{-(\pi^2p^2)/2}\big(e^{-i6\alpha\pi p}+e^{-i2\alpha\pi p}-e^{i2\alpha\pi p}-e^{i6\alpha\pi p}\big)\\
=\frac{1}{\sqrt{2\pi}}&e^{-(\pi^2(p-\frac{1}{4\alpha})^2)/2}\big(e^{-i6\alpha\pi(p-\frac{1}{4\alpha})}+e^{-i2\alpha\pi(p-\frac{1}{4\alpha})}-e^{i2\alpha\pi(p-\frac{1}{4\alpha})}-e^{i6\alpha\pi(p-\frac{1}{4\alpha})}\big)\\
&=i\sqrt{\frac{2}{\pi}}e^{-(\pi^2(p-\frac{1}{4\alpha})^2)/2}\Big(\cos(2\alpha\pi p)-\cos(6\alpha\pi p)\Big)
\end{aligned} \tag{3.21}$$

this result is very similar to the Fourier transform of $|f\rangle$ from Wenger[2003][35];

$$\sqrt{\frac{2}{\pi}}e^{-\pi^2p^2/2}\Big(\cos(2\alpha\pi p-cos(6\alpha\pi p)\Big). \tag{3.22}$$

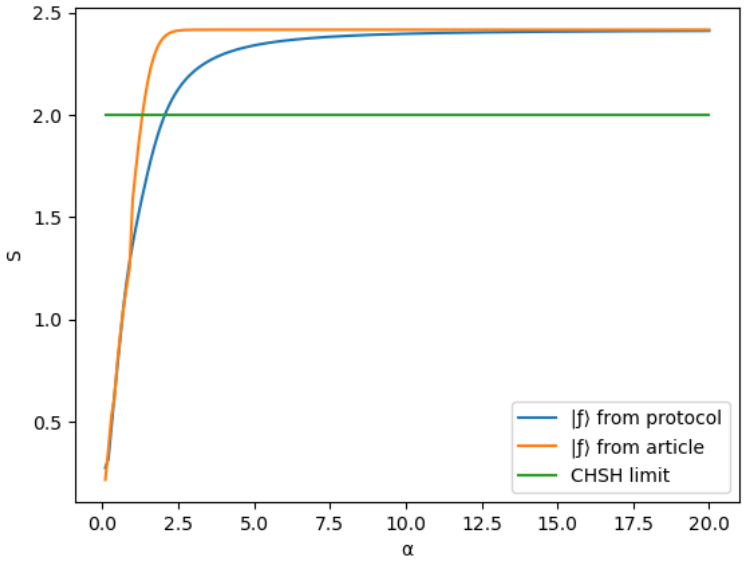

Figure 3.5: Comparison of how the value of the CHSH inequality depends on the value α for the state using $|f_{protocol}\rangle$ and $|f_{article}\rangle$. Both shows S converging toward the same value as $\alpha \to \infty$, meaning the faults introduced by the protocol become insignificant for large α. Both are plottet for $\theta = \frac{-\pi}{4}$.

Like $|f\rangle_{approx}$ in the $\hat{x}$ basis there's a prefactor of i. The fact that both the $\hat{x}$ basis and $\hat{p}$ basis of $|f\rangle$ gain a phase of i compared to the original article means the phase θ in the wavefunction $|ff\rangle + e^{i\theta}|gg\rangle$ can simply be changed to $\theta \to \theta + \pi$, or simply adding a factor of -1, which as explained above doesn't disturb our efforts to violate the CHSH inequality. Apart from the phase, the gaussian envelope function of the approximate $\hat{p}$ basis of $|f\rangle$ is shifted by $1/4\alpha$ compared to $|f\rangle$ from the article. By shifting the entire function back and comparing to $|g\rangle$, it becomes clear that it's simply $|g\rangle$ shifted in $\hat{p}$, see figure 3.4.

The CHSH inequality[7] is (see chapter 2.1.2)

$$S = |E_{xx} + E_{px} + E_{xp} - E_{pp}| \leq 2, \tag{3.23}$$

where $E_{\sigma_A \sigma_B}$ is the correlation function for a given choice of measurement basis σ for cavity A and B and is given by

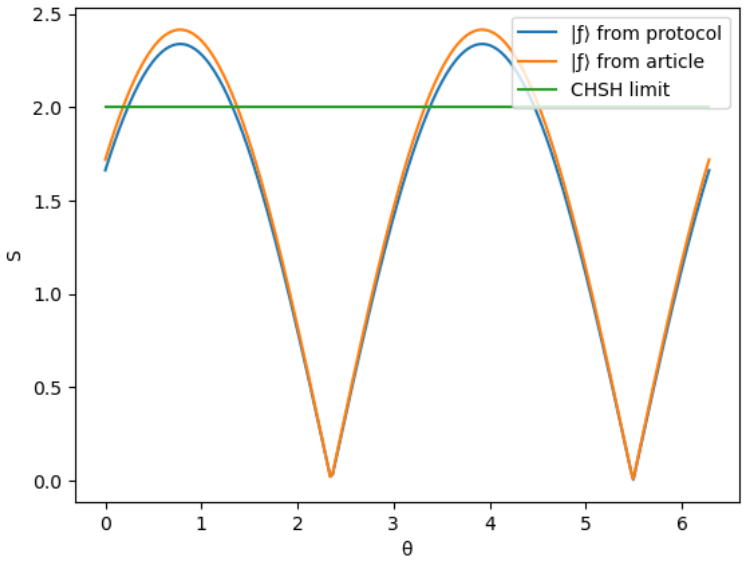

Figure 3.6: Comparison of how the value of the CHSH inequality depends on the value θ for the state using $|f_{protocol}\rangle$ and $|f_{article}\rangle$. Both share optimal values of $theta$ since the protocol introduces a factor of i for $|f\rangle$ in both the $\hat{x}$ and $\hat{p}$ basis, meaning the θ dependency of $|ff\rangle + e^{i\theta}|gg\rangle$ is shifted by π, which is of course the period of the function. Both are plottet for $\alpha = 5$

$$E = P_{++} + P_{--} - P_{+-} - P_{-+}. \tag{3.24}$$

Here $P_{(\pm\pm)}$ is a double integral with the sign denoting whether the integral is over the same-sign bins or different-sign bins of the root binning scheme for the corresponding mode;

$$P_{(\pm\pm)} = \int_{D^{\pm}} \int_{D^{\pm}} d\sigma_A d\sigma_B \Psi(\sigma_A, \sigma_B), \tag{3.25}$$

with $\Psi(\sigma_A\ , \sigma_B)$ being the wavefunction in the corresponding bases and $D^{\pm}$ denoting the group of bins to be integrated over. Since the state prepared only differs slightly from the state described in Wenger et al [2003], the value of the Bell inequality (S) unsurprisingly have similar dependencies on θ and α. In fact, since the unwanted part of $f_{protocol}$ vanishes as $\alpha \to \infty$, $S_{protocol} \to S_{article}$ for $\alpha \to \infty$ (see figure 3.5). The additional factor -1 in front of $f_{protocol}$ introduces a relative phase shift of π compared to the state of the article, however since S

as a function of θ has a periodicity of π we end up with the same we end up with similar graphs. The dependency of θ on S is shown in figure 3.6.
Apart from $|ff\rangle + e^{i\theta}|gg\rangle$, which Wenger[2003][35] revolves around, $|fg\rangle + e^{i\theta}|gf\rangle$ also yields a violation of the CHSH inequality, an important result as this doubles the chances of the protocol succeeding. This result and how it can be understood will be discussed further in the Discussion section. A plot of S as a function of θ for this state is shown in 4.5.

4 Discussion

4.1 Noise

In this chapter I will discuss the expected effects of noise and detection inefficiencies on the cavity states. The extension of the protocol to generate states with additional peaks is discussed including the trade off between higher S value and lower probability of generating the desired state.
The next section interprets the states as an entangled pair of qubits encoded in the continuous variables of the system in a subsystem decomposition adapted from the description of cluster and GKP states. Finally a few words on the choice of binning and eventual tweaks to the bins.

One of the lessons one might take away from the results above is that in order to maximize the violation of the CHSH inequality the average photon number α should be increased as much as feasible. However this information comes from a very simplistic model that includes no noise or losses and perfect generation and detection of states.
A fairly simple model could be modelling noise as our state being mixed with another noisy mode on a beamsplitter just before detection. Mathematically this is done through a convolution of the two modes, resulting in our states being 'smeared out'[23]

$$\Psi_{detected}(\hat{\sigma}) = \psi(\hat{\sigma})_{output} * \phi_{noise}(\hat{\sigma}), \tag{4.1}$$

for measurement basis $\hat{\sigma}$ ($\hat{x}$ or $\hat{p}$). For high α the well seperated array of Gaussians of the $\hat{x}$ basis should still be well defined, but one would fear that the fairly intricate trigonomic functions of the $\hat{p}$ basis would lose some of its features to this noise.
This trade-off would likely lead to an α dependency of S of rapid increase followed by slow decline, resulting in an optimization problem dependent on

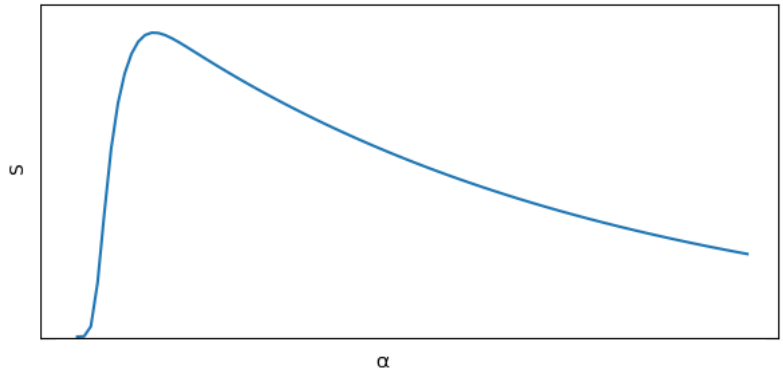

Figure 4.1: Sketch of expected results for introducing a simple model for noise, with S peaking and then slowly decaying. The position and size of the peak, and thus wether the CHSH inequality is violated, of course depends heavily on the noise in the model.

system specifics. A sketch of expected results can be seen in figure 4.1.
A way to mitigate this problem is to use squeezed light[24]. If the main problem holding back the performance of these states is the noise in the $\hat{p}$ basis while the states in the $\hat{x}$ are comparatively undisturbed, utilizing light squeezed in the $\hat{p}$ basis would improve results by sacrificing the ample resolution of the $\hat{x}$-states for more well defined $\hat{p}$-states.

4.2 Additional peaks in states

With the generated state being able to achieve a CHSH inequality above 2.4 (albeit in a perfect noiseless and lossless system) the results are promising. However, even the state of [35] that we emulate is already an approximation and truncation of states designed to reach the maximum CHSH violation of $2\sqrt{2}$, which has infinite peaks. While infinite peaks is unphysical, extending the states beyond 4 seems like an interesting prospect for improving results. Similar to [35], extending the protocol with extra steps of applying the $\sigma_x\hat{x}$ operator followed by measurements along $\hat{z}$ should, given the right $\hat{z}$ measurements, yield higher peak versions of $|f\rangle$ and $|g\rangle$. Some S values from states

N	2	4	6	8	10	12
S	1.895	2.417	2.529	2.611	2.649	2.681

Figure 4.2: Table of S values for N peaks from [wenger et al 2002], $\alpha = 7.5$.

with different number of peaks from [35] can be seen in 4.2, showing that expanding the protocol could indeed lead to a significant increase in S.
Of course, since we do additional measurements with two possible outcomes, we should expect lower odds of preparing the desired state. In fact it appears that the propability of preparing, for example, the $|f\rangle$ state with $N = 2^j$ peaks, where j is the number of iterations of the protocol applied, is

$$P(\left|f^{(2N)}\right\rangle) = \frac{1}{2^j}, \tag{4.2}$$

simply because its one of N possible outcomes, with no suggestion that multiple $\hat{z}$ measurement result combinations prepare the same state. To prepare the pre-entanglement state $|ff\rangle$ we then have the probability $\frac{1}{2^j}^2 = \frac{1}{2^{2j}}$. However, luckily, as will be discussed further below, apart from $|ff\rangle + e^{i\theta}|gg\rangle$, $|fg\rangle + e^{i\theta}|fg\rangle$ also produces a violation of the CHSH inequality in this setup, requiring the pre-entanglement result $|fg\rangle$. This doubles our chances and results in the probability

$$\frac{1}{2^{2j-1}}, \tag{4.3}$$

of preparing a desired state.
Using this method of repeatedly applying $\sigma_x\hat{x}$ will only yield states with 2^j peaks. States with number of peaks in between these might be achievable with the tools used here by using a different protocol.
Some results for 8 and 16 peaks are shown in 4.3, and some interesting observations may be inferred from them. Since the effect of the $\sigma_x\hat{x}$ operator is to split any peak in two with either same or opposite sign, we want the state after the second to last application to be one alternating in sign between peaks, denoted $|Y\rangle$ in 4.3. The last application will then split it into $|f\rangle$ for measuring $|0\rangle$ and $|g\rangle$ for $|1\rangle$. To have $|Y\rangle$ we should have a state with all peaks

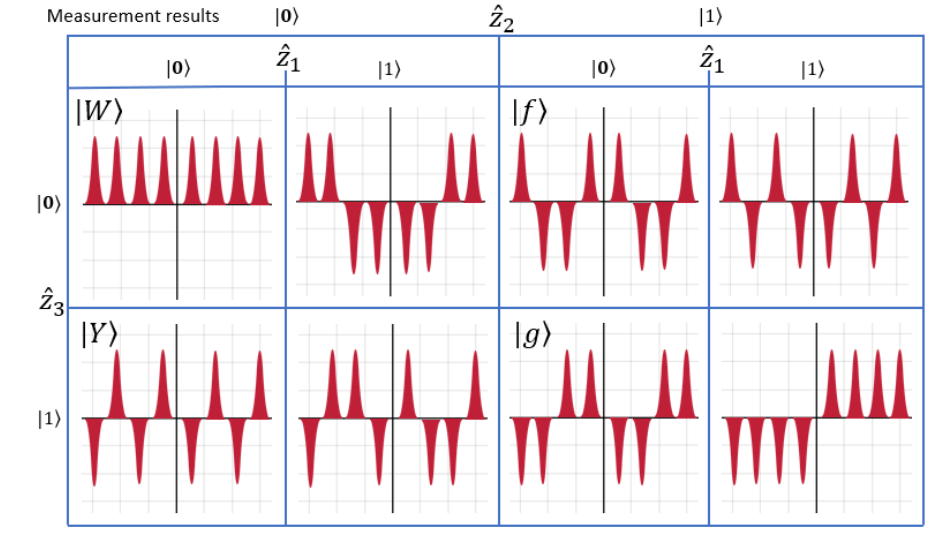

(a)

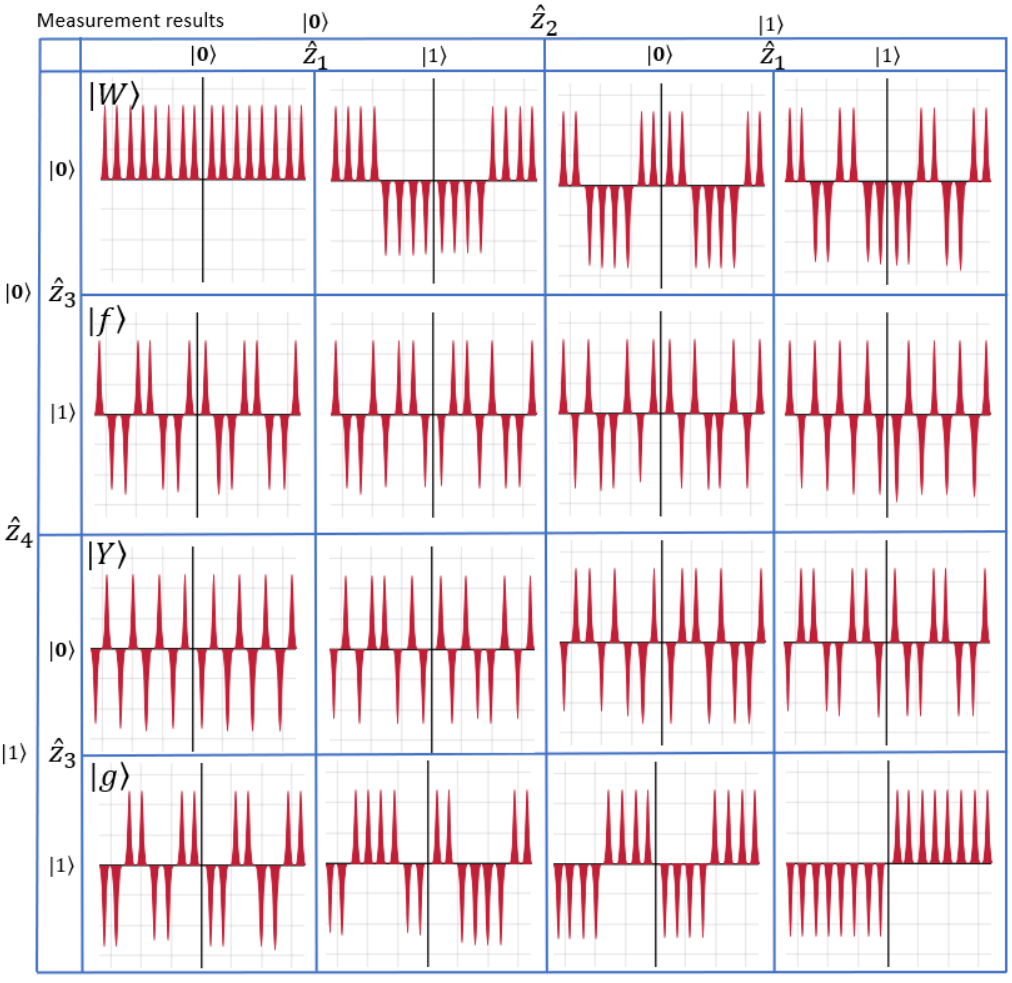

(b)

Figure 4.3: Generated states given results of $\hat{z}$ measurements during protocol. On the top and left is listed both the measurements ($\hat{z}_N$) and the result of the measurement ($|0\rangle$ or $|1\rangle$). (a) 8 peaks, corresponding to 3 $\sigma_x\hat{x}$ applications & $\hat{z}$ mesurements and (b) 16 peaks, corresponding to 4 $\sigma_x\hat{x}$ applications & $\hat{z}$ mesurements. As can be seen, regardless of number N of iterations of splitting operator $\hat{\sigma}_x\hat{x}$ and measurement of $\hat{z}$, the results required to generate $|f\rangle$ or $|g\rangle$ is to measure $|0\rangle$ for the first (N-2) measurements and $|1\rangle$ for the second to last measurement.

having the same sign, denoted $|W\rangle$ in 4.3, since measuring $|1\rangle$ will then yield $|Y\rangle$. So to prepare $|f\rangle$ or $|g\rangle$ we would like the result $|0\rangle$ for the first $(N-2)$ measurements of $\hat{z}$ to prepare $|W\rangle$, $|1\rangle$ for $\hat{z}_{N-1}$ to prepare $|Y\rangle$ and for $\hat{z}_N$ $|0\rangle$ will prepare $|f\rangle$ and $|1\rangle$ will prepare $|g\rangle$. So in this protocol $|W\rangle$ and $|Y\rangle$ are effectively precursors to $|f\rangle$ and $|g\rangle$.

4.3 Encoded Qubit

To understand why these states with this choice of binning violate the CHSH inequality it can be helpful to decompose the position wavefunction of the states. In this picture we view the position space as being partitioned into a number of smaller spaces enclosing two peaks. Each of these are divided into two, representing our binning scheme, and finally we have the modular position within our bin. We write the state as

$$|\Psi\rangle_x \to |\mathcal{L}\rangle_L \otimes |m\rangle_G \otimes |u\rangle_G \,, \tag{4.4}$$

where the subscripts indicate that the states have been divided into a logical subsystem consisting of the information of what bin we are in, this subsystem is equivalent to a qubit, and the gauge subsystem consisting of the modular position within a bin, in our case the Gaussian (-like) distribution making up the peaks, as well as the 'copies' of our two peak bin pair making up our qubit. From this it should be clear that the binning of our measurement data reduces the measurement to a measure of this qubit, while the information of qubit copy m and modular position u is disregarded.
While this in itself may be interesting it doesn't explain the violation of the CHSH inequality, since so far the state has been shown to be entangled through the states $|f\rangle$ and $|g\rangle$ and not this abstract qubit. Therefore we revisit the entangling step of the protocol within the framework of this encoded qubit.
This decomposition is fairly straightforward to envision in the x-basis, so let us start there. The $\hat{x}$ operator becomes

$$\hat{x} = \alpha \cdot \hat{\sigma}_z^{(\mathcal{L})} + 4\alpha \cdot \hat{n}^{(m)} + \hat{u}, \tag{4.5}$$

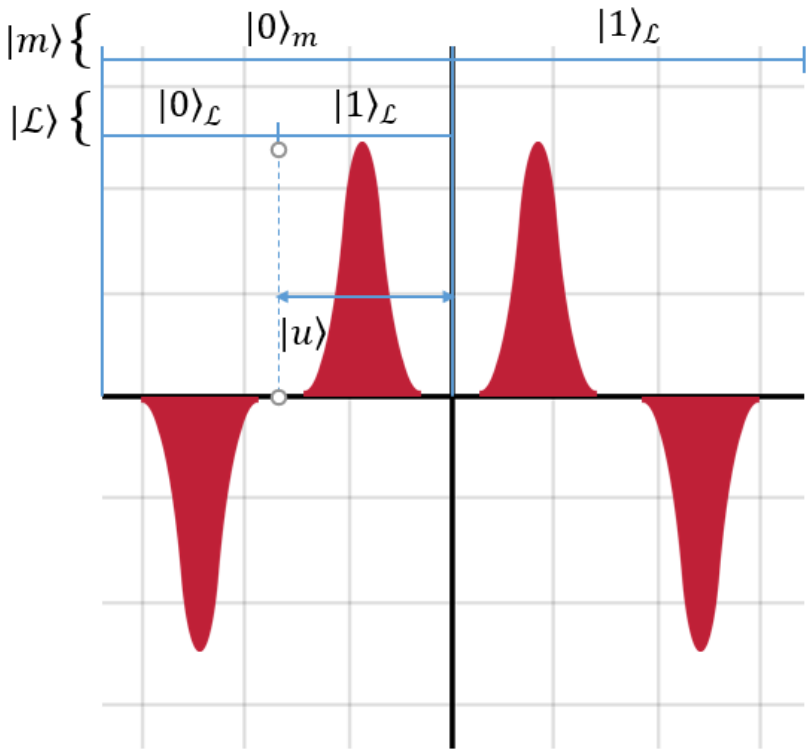

Figure 4.4: Decomposition of the $|f\rangle$ state into a qubit $|\mathcal{L}\rangle$ and two gauge states $|m\rangle$ ('copy' of the qubit) and $|u\rangle$ (modular position). Note that of the 3 subsytems only $|u\rangle$ is continuous.

for a distance between the peaks of 2α, since the width of a qubit (2 peaks) is then 4α and the distance from the middle of a copy m to the middle of a qubit bin (at the maximum of a peak) is α. $\hat{u}$ returns the modular position, $\hat{n}$ is the number operator and returns the number of the copy and $\hat{\sigma}_z = \begin{pmatrix} 1 & 0 \\ 0 & -1 \end{pmatrix}$. The entangling operator is then

$$e^{\frac{ig}{2}(\sigma_x+1)(\hat{x}_A+\hat{x}_B)t} = e^{\frac{ig}{2}(\sigma_x+1)(\alpha\cdot\hat{\sigma}_z{}_A^{(\mathcal{L})}+4\alpha\cdot\hat{n}_A^{(m)}+\hat{u}_a+\alpha\cdot\hat{\sigma}_z{}_B^{(\mathcal{L})}+4\alpha\cdot\hat{n}_B^{(m)}+\hat{u}_B)t} \tag{4.6}$$

Lets now take a look at $|g\rangle$ and $|f\rangle$ in this decomposition

$$|g\rangle = |\mathcal{L}\rangle_{|g\rangle} \otimes |m\rangle_{|g\rangle} \otimes |u\rangle_{|g\rangle} = -\Big(|0\rangle_{\mathcal{L}} + |1\rangle_{\mathcal{L}}\Big) \otimes \Big(|0\rangle_m - |1\rangle_m\Big) \otimes |u\rangle \tag{4.7}$$

$$|f\rangle = -\Big(|0\rangle_{\mathcal{L}} - |1\rangle_{\mathcal{L}}\Big) \otimes \Big(|0\rangle_m - |1\rangle_m\Big) \otimes |u\rangle \tag{4.8}$$

So the state $|ff\rangle + e^{i\theta}|gg\rangle$ becomes

$$\begin{aligned}
&\Big(|00\rangle_{\mathcal{L}} + |11\rangle_{\mathcal{L}} + |01\rangle_{\mathcal{L}} + |10\rangle_{\mathcal{L}}\Big) \\
&\otimes\Big(|00\rangle_m + |11\rangle_m - |01\rangle_m - |10\rangle_m\Big) \otimes |u\rangle_A \otimes |u\rangle_B \\
&+e^{i\theta}\cdot\Big(|00\rangle_{\mathcal{L}} + |11\rangle_{\mathcal{L}} - |01\rangle_{\mathcal{L}} - |10\rangle_{\mathcal{L}}\Big) \\
&\otimes\Big(|00\rangle_m + |11\rangle_m - |01\rangle_m - |10\rangle_m\Big) \otimes |u\rangle_A \otimes |u\rangle_B \\
&= \Big(\Phi^+_{\mathcal{L}} + \Psi^+_{\mathcal{L}}\Big) \otimes \Big(\Phi^+_m - \Psi^+_m\Big) \otimes |u\rangle_A \otimes |u\rangle_B \\
&+e^{i\theta}\cdot\Big(\Phi^+_{\mathcal{L}} - \Psi^+_{\mathcal{L}}\Big) \otimes \Big(\Phi^+_m - \Psi^+_m\Big) \otimes |u\rangle_A \otimes |u\rangle_B \\
&= \Big(\Big(1+e^{i\theta}\Big)\Phi^+_{\mathcal{L}} - \Big(1-e^{i\theta}\Big)\Psi^+_{\mathcal{L}}\Big) \otimes \Big(\Phi^+_m - \Psi^+_m\Big) \otimes |u_A u_B\rangle\,,
\end{aligned} \tag{4.9}$$

where Φ^+ and Ψ^+ of course are the bell states $\frac{1}{\sqrt{2}}(|00\rangle+|11\rangle)$ and $\frac{1}{\sqrt{2}}(|01\rangle+|10\rangle)$ respectively. It is worth noting that the logical qubits are entangled only with each other and not the gauge states.
So the correlations for both modes in the $\hat{x}$-basis becomes

$$
\begin{aligned}
&\langle \Psi_{xx} | \Psi_{xx} \rangle \\
&= \Big(\big(1 + e^{-i\theta}\big)\Phi^+_{\mathcal{L}} - \big(1 - e^{-i\theta}\big)\Psi^+_{\mathcal{L}} \Big) \Big(\big(1 + e^{i\theta}\big)\Phi^+_{\mathcal{L}} - \big(1 - e^{i\theta}\big)\Psi^+_{\mathcal{L}} \Big) \\
&\otimes \Big(\Phi^+_m - \Psi^+_m \Big)^\dagger \Big(\Phi^+_m - \Psi^+_m \Big) \otimes \langle u_A u_B | u_A u_B \rangle \\
&\propto \cos\theta
\end{aligned}
\tag{4.10}
$$

Similar to the result in [35]. I have not been able to complete the calculation for the $\hat{p}$-basis, but I expect the results to be similar to [35] as well, i.e.

$$\langle \Psi_{pp} | \Psi_{pp} \rangle \propto \cos\theta \tag{4.11}$$

$$\langle \Psi_{xp} | \Psi_{xp} \rangle \propto \sin\theta \tag{4.12}$$

$$\langle \Psi_{px} | \Psi_{px} \rangle \propto \sin\theta. \tag{4.13}$$

This would mathematecally explain why $\theta = -\frac{\pi}{4}$ maximizes S, for ∞ peaks at least, since the derived expression for S in [Wenger 2002] is

$$S = |\cos(\theta)\Big(V^2 + W^2\Big) - 2\sin(\theta)VW| \leq 2, \tag{4.14}$$

where V and W are the normalized overlaps of $|f\rangle$ and $|g\rangle$ in the $\hat{x}$ and $\hat{p}$-basis respectively.

The decomposition used above is adapted from the description of two families of continuous variable states proposed as potential foundations for quantum computing, CV cluster states and among them GKP states[13][26]. The idea is to have an array of identical qubits encoded in the states. These copies can be used to shield the qubit from noise and decoherence, thus making the system much more stable.

Cluster states do tend to have unwanted correlations between the encoded qubit and the gauge subsystems making them less effective. This can be solved by including GKP states in the entanglement as these states can 'unzip' the encoded qubit from the gauge subsystems, making it the states much more desireable[26].

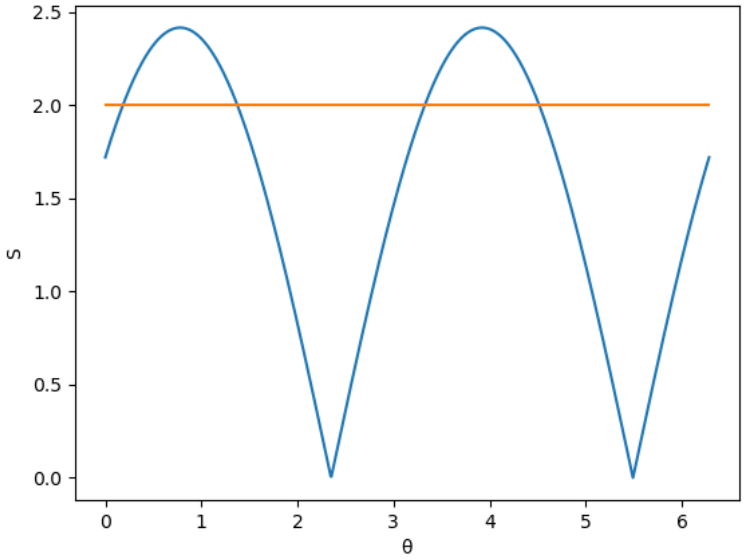

Figure 4.5: S as a function of θ for $|fg\rangle + e^{i\theta}|gf\rangle$ for $\alpha = 5$

This interpretation of the states generated by the protocol described in this report highlights the potential for similar states of an extended protocol to higher number of peaks to be useful in error correction within quantum computing.

4.3.1 $|fg\rangle + e^{i\theta}|gf\rangle$

With this interpretation of the choice of binning and states boiling down to an encoded qubit, one might ask that if the even entanglement $|ff\rangle + e^{i\theta}|gg\rangle$ produces a violation of the CHSH inequality, could other combinations violate CHSH too? As it turns out the answer is yes, the state $|fg\rangle + e^{i\theta}|gf\rangle$ have the same α and θ dependencies for S (see figure 4.5) and as the periodicity in θ of π shows both $|ff\rangle - e^{i\theta}|gg\rangle$ and $|fg\rangle - e^{i\theta}|gf\rangle$ are suitable states as well.
The phase bit not changing the S value of states means the random sign introduced here by the protocol does not limit our efficiency.The even-odd parity bit of the encoded logical qubit being interchangable, however, means the protocol doubles in efficiency with now having two usable outcomes instead of one.

4.4 Choice of binning

The states used are constructed specifically to work with the root binning scheme, so changing the overall binning scheme is unlikely to improve results. However with noise, losses and detector inefficiency likely to distort the shape of the wave functions, it is possible that tweaking the bins and their edges could improve correlations.
This optimization could be done after the fact, finding the best set of bins from measurement data. However this would require comparing results via conventional means, which for practical use in quantum communication of course would mean giving up your quantum key. Not exactly ideal, so bins would have to be agreed ahead of time.

5 Conclusion

Through the interaction of superconducting qubits with microwave cavities a protocol for producing continuous variable states violating the CHSH inequality has been proposed. It's based on the scheme proposed in Wenger [2002][35], reproducing the states down to a position dependent phase on one term of the entangled superposition. In terms of the subsystem decomposition of the state, this phase can be understood to stem from the interaction between the entangling operator and the modular position subsystem.

The protocol is not deterministic but has a $\frac{1}{8}$ chance of succeeding, however since preparing measurements on the interacting qubits tell whether the protocol was successful only successfully prepared states need be considered when calculating the inequality. In a theoretical with no noise and loss and perfect generation and detection the states have an S value of almost 2.5. Of course a realistic setup with all these included will lead to lower S values, but this can be mitigated either by utilizing squeezed light to shield especially against noise in the intricate $\hat{p}$-basis wavefunctions, or by extending the protocol to generate states with additional peaks than the 4 of states produced by this protocol.

An extended protocol would have a success rate of $\frac{2}{N^2}$ where N is number of peaks of the generated states since not only $|ff\rangle + e^{i\theta}|gg\rangle$ but also $|fg\rangle + e^{i\theta}|gf\rangle$ is found to violate the CHSH inequality for appropriate choice of phase θ. This again can be understood in the subsystem decomposition view of the states as having different states of the encoded logical qubit.

6 Appendixes

6.1 Early attempts

Before figuring out a protocol that worked for generating continuous variable states violating the CHSH inequality, several other attempts were made unsuccessfully. Here follows a summation.

6.1.1 Kerr induced multi component cat states

Initially the idea was to utilize multi component cat states generated through the interaction of a microwave cavity and a Kerr medium as a basis[18]. Partially as a learning experiance, the first attempts involved rather simple setups using a single source and beamsplitter and simple binning scheme with the full expectation not to achieve a violation of the CHSH inequality. The team behind the article detailing the Kerr induced states were able to prepare 4 component cat states, so this seemed like a good starting point. The binning scheme I used was a simple positive-negative scheme, i.e. results ≥ 0 were given the value 1 and results ≤ 0 give -1. The states considered were

$$|\Psi_{'square'}\rangle = \sum_{n=0}^{3} \frac{1}{2} \left| e^{i(2n+1)\pi/4}\alpha \right\rangle \tag{6.1}$$

$$|\Psi_{'diamond'}\rangle = \sum_{n=0}^{3} \frac{1}{2} \left| e^{in\pi/2}\alpha \right\rangle \tag{6.2}$$

$$|\Psi_{'triangle'}\rangle = \sum_{n=0}^{2} \frac{1}{\sqrt{3}} \left| e^{i2n\pi/3}\alpha \right\rangle . \tag{6.3}$$

After being split on a $50/50$ beamsplitter with a vacuum state, these states become

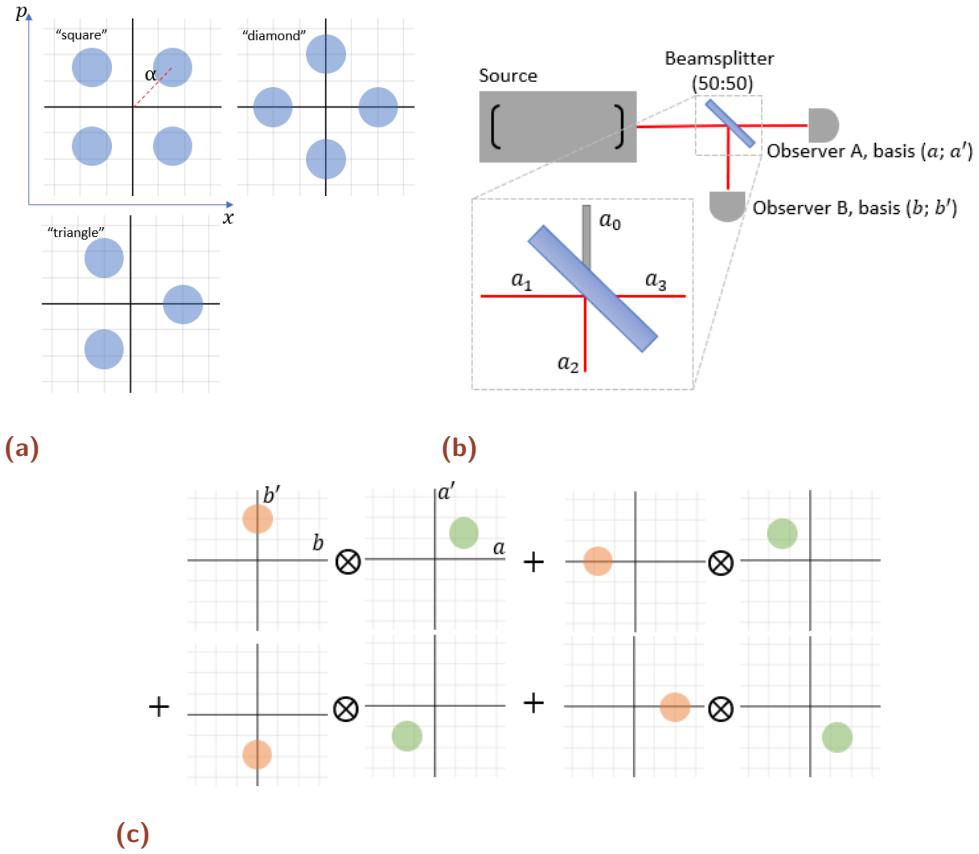

Figure 6.1: (a) Phase space visualization of the multicomponent cat states. (b) very simple setup of source, beamsplitter and observers.(c) resulting state of splitting the $'square'$ state on a beamsplitter.

$$|0\rangle_0 |\Psi_{'square'}\rangle \rightarrow \frac{1}{2}\sum_{n=0}^{3} \left| e^{i(2n+3)\pi/4}\frac{\alpha}{\sqrt{2}} \right\rangle_2 \left| e^{i(2n+1)\pi/2}\frac{\alpha}{\sqrt{2}} \right\rangle_3 \tag{6.4}$$

$$|0\rangle_0 |\Psi_{'diamond'}\rangle \rightarrow \frac{1}{2}\sum_{n=0}^{3} \left| e^{i(n+1)\pi/2}\frac{\alpha}{\sqrt{2}} \right\rangle_2 \left| e^{in\pi/2}\frac{\alpha}{\sqrt{2}} \right\rangle_3 \tag{6.5}$$

$$|0\rangle_0 |\Psi_{'triangle'}\rangle \rightarrow \frac{1}{\sqrt{3}}\sum_{n=0}^{3} \left| e^{i(4n+3)\pi/6}\frac{\alpha}{\sqrt{2}} \right\rangle_2 \left| e^{i2n\pi/3}\frac{\alpha}{\sqrt{2}} \right\rangle_3 \tag{6.6}$$

see figure 6.1. These states are entangled, with as many terms as there are components in the initial states, however calculating the CHSH inequality with the simple binning scheme described above leads to no violations for either state. Assuming large α (so that states are orthogonal), a simple estimation of S can be made simply by 'counting' the correlations from the phase space plot, counting each coherent component as 1 and placing them in appropriate bins, see figure 6.1, the correlations are calculated as

$$E_{\sigma_a\sigma_b} = P_{+\sigma_a+\sigma_b} + P_{-\sigma_a-\sigma_b} - P_{+\sigma_a-\sigma_b} - P_{-\sigma_a+\sigma_b}, \tag{6.7}$$

with $P_{\pm\sigma_a\pm\sigma_b}$ being the probability of measuring a given bin for a given measurement basis. The correlations become

$$E_{ab} = \frac{1}{4}\left(\frac{3}{2} + \frac{3}{2} - \frac{1}{2} - \frac{1}{2}\right) = \frac{1}{2} \tag{6.8}$$

$$E_{ab'} = \frac{1}{4}\left(\frac{3}{2} + \frac{3}{2} - \frac{1}{2} - \frac{1}{2}\right) = \frac{1}{2} \tag{6.9}$$

$$E_{a'b} = \frac{1}{4}\left(\frac{1}{2} + \frac{1}{2} - \frac{3}{2} - \frac{3}{2}\right) = -\frac{1}{2} \tag{6.10}$$

$$E_{a'b'} = \frac{1}{4}\left(\frac{3}{2} + \frac{3}{2} - \frac{1}{2} - \frac{1}{2}\right) = \frac{1}{2}, \tag{6.11}$$

so that S becomes

$$S = |\frac{1}{2} + \frac{1}{2} + \frac{1}{2} - \left(-\frac{1}{2}\right)| = 2 \leq 2, \tag{6.12}$$

so the inequality holds.
A thorough calculation of S shows that this is in fact the upper limit on S as can be seen in figure 6.2 (a) and (b).

6.1.2 Reverse engineering $|ff\rangle + e^{i\theta}|gg\rangle$

Following these early attempts described above, the decision was made to attempt to recreate entangled states that had already been shown to violate the CHSH inequality theoretically and the choice fell on the states of Wenger[2002][35] since these states also consisted of multiple coherent states, albeit in arrays rather than radially distributed in phase space, and as such seemed feasible to reproduce with the tools at hand, although later the method of utilizing an interaction with a Kerr medium was discarded.
First an attempt was made to find unitary 2x2 operators that could disentangle $|ff\rangle + e^{i\theta}|gg\rangle$, since the Hermetian conjugate of the operator would then be

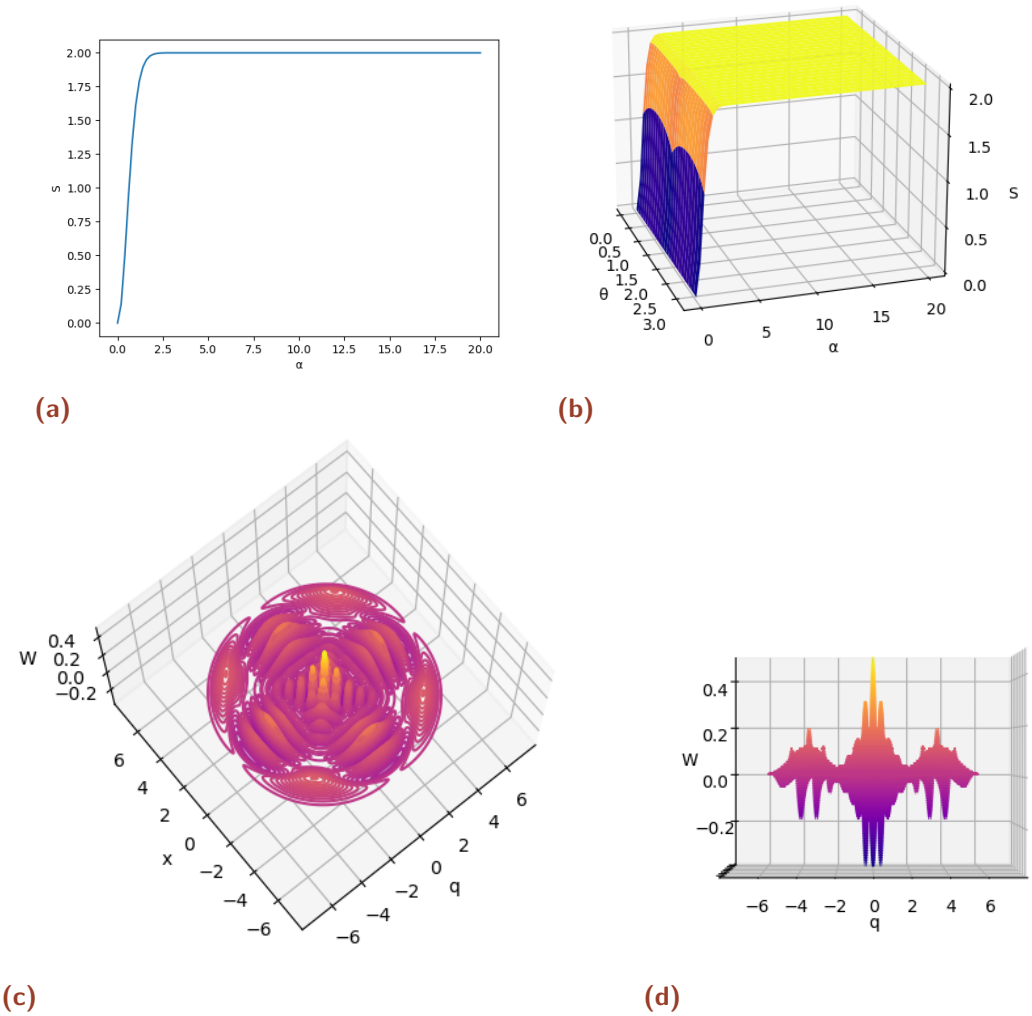

Figure 6.2: (a) CHSH inequality for a 4 component cat state as a function of mean photon number α for an angle between observer basis of measurement of $\frac{\pi}{4}$. (b) The same plot extended to all angles, as can be seen some angles may approach the maximum of 2 faster, but non violate the inequality, as expected. (c) & (d) Wigner function of 4 component cat state, showing multiple negative regions as well as a lot of symmetry.

able to entangle the found state into $|ff\rangle + e^{i\theta}|gg\rangle$. A 2x2 unitary matrix has the general form

$$\begin{bmatrix} a & b \\ -e^{i\phi}b^* & e^{i\phi}a^* \end{bmatrix}, \tag{6.13}$$

with $|a|^2 + |b|^2 = 1$. This matrix depends on 4 parameters; ϕ, the phases of a and b and $\frac{a}{b}$.
To check whether a given operator has disentangled the state, we use the Von Neumann entropy, defined as

$$S = -\operatorname{Tr}\{\rho \ln \rho\}, \tag{6.14}$$

with Tr being the trace and ρ is the density matrix of the state. The Von Neumann of a state has the property that it is 0 only if the state is a pure state, meaning that we can use it as a measure for whether the state is entangled or not. So with a 4 variable operator and a scalar variable to minimize (or at least minimize the argument of), this has turned into an optimization problem.
The python optimization package Optuna[1] was used to search for parameters generating $S = 0$, however after some 100.000 trials no such parameters were found. After this attempt the $\sigma_x\hat{x}$ operator derived for a SC qubit-MW resonator interaction by another masters student presented itself as an interesting prospect for a nonlinear operator to induce entanglement and turned out succesful.

6.2 Superfluous states generated by the protocol

As stated in the results chapter, the initial 2 applications of single resonator $\sigma_x\hat{x}$ operators can lead to 4 different states, $|f\rangle$, $|g\rangle$, $|Y\rangle$ and $|W\rangle$, and with 2 resonators this means 16 different possible outcomes. Only four of these ($|ff\rangle, |gg\rangle, |fg\rangle, |gf\rangle$) violate the CHSH inequality, albeit for different values

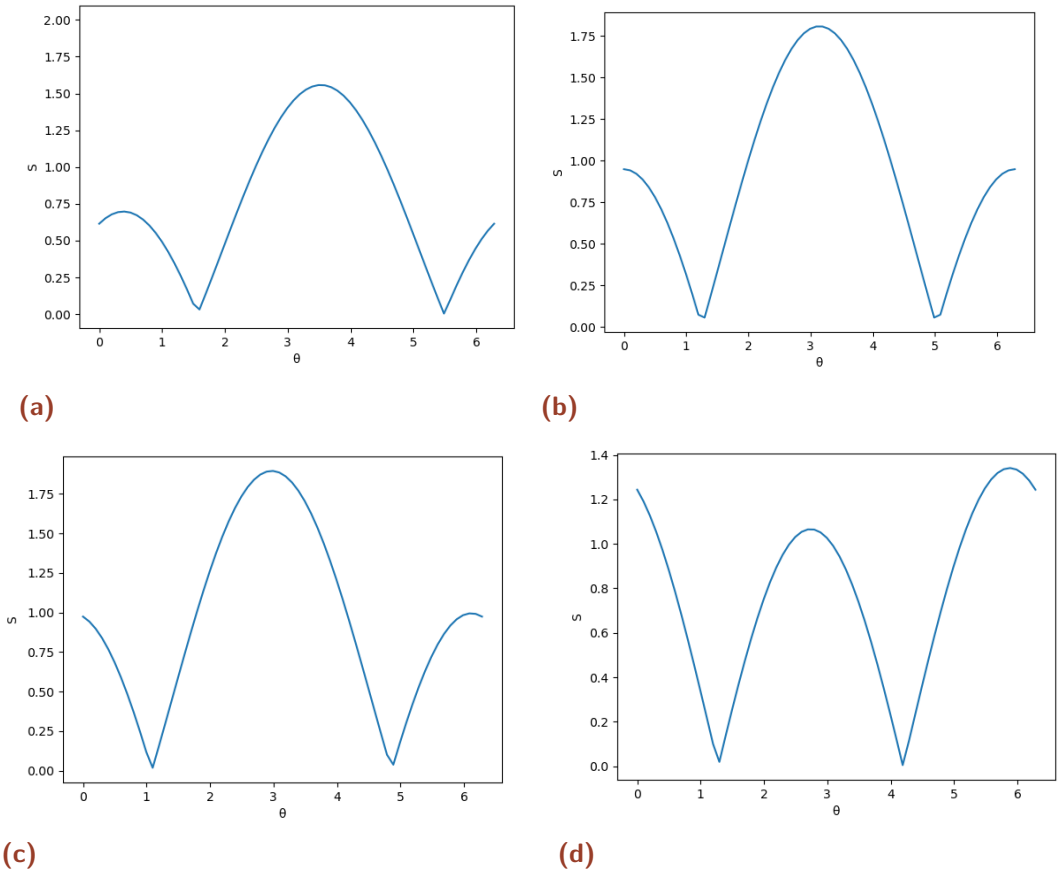

Figure 6.3: Plots of S as a function of θ at $\alpha = 5$ for the states found not to violate the CHSH inequality, the $\hat{x}$ basis wavefunction can be seen in 3.2; (a) $|WW\rangle + e^{i\theta}|YY\rangle$, equivalent to $|YY\rangle + e^{-i\theta}|WW\rangle$. (b) $|YW\rangle + e^{i\theta}|WY\rangle$, $|WY\rangle + e^{-i\theta}|YW\rangle$ has similar results. $|fW\rangle + e^{i\theta}|gY\rangle$ with $|gY\rangle + e^{i\theta}|fW\rangle$, $|Wf\rangle + e^{i\theta}|Yg\rangle$ and $|Yg\rangle + e^{i\theta}|Wf\rangle$ all having similar result, albeit some with $-\theta$ substituted for θ. (d) $|fY\rangle + e^{i\theta}|gW\rangle$, similar to the previous plot this is also representative of $|gW\rangle + e^{i\theta}|fY\rangle$, $|Wg\rangle + e^{i\theta}|Yf\rangle$ and $|Yf\rangle + e^{i\theta}|Wg\rangle$.

of θ, but theit S values was plotted non the less hoping to find an unexpected inequality violation. The plots can be seen in figure 6.3.

7 Bibliography

[1] Takuya Akiba, Shotaro Sano, Toshihiko Yanase, Takeru Ohta, and Masanori Koyama. „Optuna: A Next-generation Hyperparameter Optimization Framework“. In: *CoRR* abs/1907.10902 (2019). arXiv: 1907.10902.

[2] Hedwig Born Albert Einstein Max Born. *The Born-Einstein Letters: Correspondence Between Albert Einstein and Max and Hedwig Born from 1916-1955, with Commentaries by Max Born*. Macmillan, 1971.

[3] J. S. Bell. „On the Einstein Podolsky Rosen paradox“. In: *Physics Physique Fizika* 1 (3 Nov. 1964), pp. 195–200.

[4] Charles H. Bennett and Gilles Brassard. „Quantum cryptography: Public key distribution and coin tossing“. In: *Theoretical Computer Science* 560 (2014). Theoretical Aspects of Quantum Cryptography – celebrating 30 years of BB84, pp. 7–11.

[5] Samantha Buck, Robin Coleman, and Hayk Sargsyan. *Continuous Variable Quantum Algorithms: an Introduction*. 2021. arXiv: 2107.02151 [quant-ph].

[6] E. G. Cavalcanti, C. J. Foster, M. D. Reid, and P. D. Drummond. „Bell Inequalities for Continuous-Variable Correlations“. In: *Phys. Rev. Lett.* 99 (21 Nov. 2007), p. 210405.

[7] John F. Clauser, Michael A. Horne, Abner Shimony, and Richard A. Holt. „Proposed Experiment to Test Local Hidden-Variable Theories“. In: *Phys. Rev. Lett.* 23 (15 Oct. 1969), pp. 880–884.

[8] John M. Donohue, Megan Agnew, Jonathan Lavoie, and Kevin J. Resch. „Coherent Ultrafast Measurement of Time-Bin Encoded Photons“. In: *Phys. Rev. Lett.* 111 (15 Oct. 2013), p. 153602.

[9] A. Einstein, B. Podolsky, and N. Rosen. „Can Quantum-Mechanical Description of Physical Reality Be Considered Complete?“ In: *Phys. Rev.* 47 (10 May 1935), pp. 777–780.

[10] M. D. Eisaman, J. Fan, A. Migdall, and S. V. Polyakov. „Invited Review Article: Single-photon sources and detectors“. In: *Review of Scientific Instruments* 82.7 (2011), p. 071101. eprint: `https://doi.org/10.1063/1.3610677`.

[11] Raúl Garcıa-Patrón, Jaromır Fiurá šek, and Nicolas J. Cerf. „Loophole-free test of quantum nonlocality using high-efficiency homodyne detectors“. In: *Phys. Rev. A* 71 (2 Feb. 2005), p. 022105.

[12] Nicolas Gisin, Grégoire Ribordy, Wolfgang Tittel, and Hugo Zbinden. „Quantum cryptography“. In: *Rev. Mod. Phys.* 74 (1 Mar. 2002), pp. 145–195.

[13] Daniel Gottesman, Alexei Kitaev, and John Preskill. „Encoding a qubit in an oscillator“. In: *Phys. Rev. A* 64 (1 June 2001), p. 012310.

[14] Robert Hadfield. „Single-photon detectors for optical quantum information applications“. In: *Nature Photonics* 3 (Dec. 2009).

[15] H. Hansen, T. Aichele, C. Hettich, P. Lodahl, A. I. Lvovsky, J. Mlynek, and S. Schiller. „Ultrasensitive pulsed, balanced homodyne detector:application to time-domain quantum measurements“. In: *Opt. Lett.* 26.21 (Nov. 2001), pp. 1714–1716.

[16] B. Hensen, H. Bernien, A. Dréau, *et al.* „Loophole-free Bell inequality violation using electron spins separated by 1.3 kilometres“. In: *Nature* 526 (Oct. 2015).

[17] J.R. Johansson, P.D. Nation, and Franco Nori. „QuTiP 2: A Python framework for the dynamics of open quantum systems“. In: *Computer Physics Communications* 184.4 (2013), pp. 1234–1240.

[18] Gerhard Kirchmair, Brian Vlastakis, Zaki Leghtas, Simon Nigg, Hanhee Paik, Eran Ginossar, Mazyar Mirrahimi, Luigi Frunzio, Steven Girvin, and Robert Schoelkopf. „Observation of quantum state collapse and revival due to the single-photon Kerr effect“. In: *Nature* 495 (Mar. 2013), pp. 205–9.

[19] Hyukjoon Kwon and Hyunseok Jeong. „Violation of the Bell–Clauser-Horne-Shimony-Holt inequality using imperfect photodetectors with optical hybrid states“. In: *Phys. Rev. A* 88 (5 Nov. 2013), p. 052127.

[20] Seth Lloyd and Samuel L. Braunstein. „Quantum Computation over Continuous Variables“. In: *Phys. Rev. Lett.* 82 (8 Feb. 1999), pp. 1784–1787.

[21] Wen-Long Ma, Shruti Puri, Robert J. Schoelkopf, Michel H. Devoret, S.M. Girvin, and Liang Jiang. „Quantum control of bosonic modes with superconducting circuits“. In: *Science Bulletin* 66.17 (2021), pp. 1789–1805.

[22] I. Marcikic, H. de Riedmatten, W. Tittel, H. Zbinden, M. Legré, and N. Gisin. „Distribution of Time-Bin Entangled Qubits over 50 km of Optical Fiber“. In: *Phys. Rev. Lett.* 93 (18 Oct. 2004), p. 180502.

[23] G. Mauro D'Ariano, Matteo G. A. Paris, and Massimiliano F. Sacchi. „Quantum Tomography“. In: *arXiv e-prints*, quant-ph/0302028 (Feb. 2003), quant–ph/0302028. arXiv: quant-ph/0302028 [quant-ph].

[24] Moritz Mehmet, Stefan Ast, Tobias Eberle, Sebastian Steinlechner, Henning Vahlbruch, and Roman Schnabel. „Squeezed light at 1550 nm with a quantum noise reduction of 12.3 dB“. In: *Opt. Express* 19.25 (Dec. 2011), pp. 25763–25772.

[25] Martin R. Ostermeyer and Nino Walenta. „On the implementation of a deterministic secure coding protocol using polarization entangled photons“. In: *Optics Communications* 281 (2008), pp. 4540–4544.

[26] Giacomo Pantaleoni, Ben Q. Baragiola, and Nicolas C. Menicucci. „Hidden qubit cluster states“. In: *Phys. Rev. A* 104 (1 July 2021), p. 012431.

[27] John Preskill. „Lecture Notes for Physics Quantum Information and Computation“. In: (Sept. 1998).

[28] MA Rowe, David Kielpinski, V Meyer, Charles Sackett, Wayne Itano, C Monroe, and D Wineland. „Experimental violation of a Bell's inequality with efficient detection“. In: *Nature* 409 (Mar. 2001), pp. 791–4.

[29] Jr. au2 Samuel J. Lomonaco and Louis H. Kauffman. *A Continuous Variable Shor Algorithm*. 2004. arXiv: quant-ph/0210141 [quant-ph].

[30] Oliver Thearle, Jiri Janousek, Seiji Armstrong, *et al.* „Violation of Bell's Inequality Using Continuous Variable Measurements“. In: *Phys. Rev. Lett.* 120 (4 Jan. 2018), p. 040406.

[31] Andreas Wallraff, David Schuster, A Blais, L Frunzio, R Huang, J Majer, S Kumar, Steven Girvin, and R Schoelkopf. „Strong coupling of a single photon to a superconducting qubit using circuit quantum electrodynamics“. In: *Nature* 431 (Oct. 2004), pp. 162–7.

[32] YangMing Wang. *Circuit QED Project Report*. Aug. 2021.

[33] Gregor Weihs, Thomas Jennewein, Christoph Simon, Harald Weinfurter, and Anton Zeilinger. „Violation of Bell's Inequality under Strict Einstein Locality Conditions“. In: *Phys. Rev. Lett.* 81 (23 Dec. 1998), pp. 5039–5043.

[34] Wang Wen-Feng, Sun Xin-Yuan, and Xiaobing Luo. „Generation of Cluster-Type Entangled Coherent States via Cross-Kerr Nonlinearity“. In: *Chinese Physics Letters* 25 (Mar. 2008), p. 839.

[35] Jérôme Wenger, Mohammad Hafezi, Frédéric Grosshans, Rosa Tualle-Brouri, and Philippe Grangier. „Maximal violation of Bell inequalities using continuous-variable measurements“. In: *Phys. Rev. A* 67 (1 Jan. 2003), p. 012105.

[36] Jing Wu and Quntao Zhuang. „Continuous-Variable Error Correction for General Gaussian Noises“. In: *Phys. Rev. Applied* 15 (3 Mar. 2021), p. 034073.

[37] Lixing You. „Superconducting Nanowire Single-Photon Detectors for Quantum Information“. In: (May 2020).

[38] Marcin Zwierz. „Quantum Information Processing with Continuous Variables and Atomic Ensembles“. In: (Feb. 2011).